Postnatal development of the entorhinal cortex: A stereological study in macaque monkeys

Olivia Piguet[1] | Loïc J Chareyron[2] | Pamela Banta Lavenex[1,3] | David G Amaral[4,5] | Pierre Lavenex[1,2]

[1]Laboratory of Brain and Cognitive Development, Institute of Psychology, University of Lausanne, Lausanne

[2]Department of Medicine, University of Fribourg, Fribourg

[3]Faculty of Psychology, Swiss Distance University, Brig

[4]Department of Psychiatry and Behavioral Sciences, MIND Institute, University of California, Davis, California

[5]California National Primate Research Center, University of California, Davis, California

Correspondence
Pierre Lavenex, Laboratory of Brain and Cognitive Development, Institute of Psychology, University of Lausanne, 1015 Lausanne, Switzerland.
Email: pierre.lavenex@unil.ch

Funding information
California National Primate Research Center, Grant/Award Number: OD011107; National Institutes of Health, Grant/Award Numbers: MH041479, NS16980; Schweizerischer Nationalfonds zur Förderung der Wissenschaftlichen Forschung, Grant/Award Numbers: 310030_143956, P00A-106701, PP00P3-124536

Peer Review
The peer review history for this article is available at https://publons.com/publon/10.1002/cne.24897.

Abstract

The entorhinal cortex is the main gateway for interactions between the neocortex and the hippocampus. Distinct regions, layers, and cells of the hippocampal formation exhibit different profiles of structural and molecular maturation during postnatal development. Here, we provide estimates of neuron number, neuronal soma size, and volume of the different layers and subdivisions of the monkey entorhinal cortex (Eo, Er, Elr, Ei, Elc, Ec, Ecl) during postnatal development. We found different developmental changes in neuronal soma size and volume of distinct layers in different subdivisions, but no changes in neuron number. Layers I and II developed early in most subdivisions. Layer III exhibited early maturation in Ec and Ecl, a two-step/early maturation in Ei and a late maturation in Er. Layers V and VI exhibited an early maturation in Ec and Ecl, a two-step and early maturation in Ei, and a late maturation in Er. Neuronal soma size increased transiently at 6 months of age and decreased thereafter to reach adult size, except in Layer II of Ei, and Layers II and III of Ec and Ecl. These findings support the theory that different hippocampal circuits exhibit distinct developmental profiles, which may subserve the emergence of different hippocampus-dependent memory processes. We discuss how the early maturation of the caudal entorhinal cortex may contribute to path integration and basic allocentric spatial processing, whereas the late maturation of the rostral entorhinal cortex may contribute to the increased precision of allocentric spatial representations and the temporal integration of individual items into episodic memories.

KEYWORDS

allocentric spatial memory, episodic memory, hippocampal formation, infantile amnesia, RRID:SCR_000696, California National Primate Research Center Analytical and Resource Core, RRID:SCR_002526, Stereo Investigator, RRID:SCR_002865, SPSS, RRID:SCR_014199, Adobe Photoshop, *Macaca mulatta*, medial temporal lobe, object memory, path integration

1 | INTRODUCTION

The entorhinal cortex constitutes the main interface for bidirectional interactions between the neocortex and the hippocampal formation (i.e., which includes the dentate gyrus, hippocampus proper [CA3, CA2, CA1], subiculum, presubiculum, parasubiculum, and entorhinal cortex) in support of spatial and episodic memory functions (Amaral & Lavenex, 2007; Lavenex & Amaral, 2000; Witter, Doan, Jacobsen, Nilssen, & Ohara, 2017). Previous research has shown that distinct regions, layers and cells of the monkey hippocampal formation exhibit different profiles of structural and molecular changes during early postnatal development (Favre, Banta Lavenex, & Lavenex,

2012a, 2012b; Jabès, Banta Lavenex, Amaral, & Lavenex, 2010, 2011; Lavenex, Banta Lavenex, & Amaral, 2004, 2007; Lavenex, Banta Lavenex, & Favre, 2014). The protracted period of neuron addition and maturation in the dentate gyrus is accompanied by the late maturation of specific layers and structures in hippocampal regions that are located downstream from the dentate gyrus, in particular CA3. In contrast, distinct layers of hippocampal regions that receive direct projections from the entorhinal cortex, in particular CA1, exhibit a comparatively earlier maturation. The subiculum, presubiculum, parasubiculum, and CA2, which are highly interconnected with subcortical structures, mature even earlier. Together with studies of the development of human spatial memory (Ribordy, Jabès, Banta Lavenex, & Lavenex, 2013; Ribordy Lambert, Lavenex, & Banta Lavenex, 2015, 2016), these findings suggested that the differential maturation of distinct hippocampal circuits might underlie the emergence of different hippocampus-dependent memory processes (Lavenex & Banta Lavenex, 2013). This theory was based on the emerging principle that specific types of information processing are subserved by different neuronal circuits within the medial temporal lobe (Kesner, Lee, & Gilbert, 2004; Kesner & Rolls, 2015; Knierim & Neunuebel, 2016; Knierim, Neunuebel, & Deshmukh, 2014; Witter & Moser, 2006). To date, however, the developmental profiles of the different layers of the seven subdivisions of the monkey entorhinal cortex have yet to be determined, information that is critical to more fully understand the functional maturation of this memory system.

1.1 | Organization of the entorhinal cortex

The monkey entorhinal cortex comprises seven subdivisions (Amaral, Insausti, & Cowan, 1987; Piguet, Chareyron, Banta Lavenex, Amaral, & Lavenex, 2018): Eo, the olfactory subdivision; Er, the rostral subdivision; El, the lateral subdivision, which comprises the lateral rostral (Elr) and lateral caudal (Elc) subdivisions; Ei, the intermediate subdivision; Ec, the caudal subdivision; and Ecl, the caudal limiting subdivision. A simplified description of the connectivity of the entorhinal cortex indicates that its superficial Layers II and III represent the main entryways for much of the cortical information to be processed by the hippocampal formation, although the deep Layers V and VI also contribute minor projections to the dentate gyrus and the hippocampus (Witter, Van Hoesen, & Amaral, 1989). In contrast, its deep layers are the main recipients of projections from the CA1 region of the hippocampus and the subiculum, and provide the main conduit by which information is sent back to the neocortex. In monkeys, the perirhinal and parahippocampal cortices provide about two-thirds of the cortical projections reaching the entorhinal cortex, but these projections are preferentially directed toward different subdivisions (Suzuki & Amaral, 1994). The projections from the perirhinal cortex terminate predominantly in the rostral two-thirds of the entorhinal cortex, in particular Eo, Er, Elr, Ei, and Elc. The projections from the parahippocampal cortex, in contrast, terminate predominantly in the caudal two-thirds of the entorhinal cortex, in particular Ei, Ec, and Ecl. Other cortical projections to the entorhinal cortex originate in the temporal lobes, frontal cortex, insula, cingulate and retrosplenial cortices, and terminate preferentially in different subdivisions (Insausti & Amaral, 2008; Insausti, Amaral, & Cowan, 1987). Projections from the insula, the orbitofrontal cortex, and the anterior cingulate cortex are directed predominantly toward rostral areas Eo, Er, Elr, and the rostral part of Ei, whereas projections from the retrosplenial cortex and the superior temporal gyrus are directed predominantly toward caudal areas Ec and Ecl, and the caudal part of Ei. Projections from the amygdala are directed toward the rostral subdivisions of the entorhinal cortex, including Eo, Er, Elr, and the rostral parts of Ei and Elc, with essentially no amygdala projections to the caudal areas Ec and Ecl (Pitkänen, Kelly, & Amaral, 2002).

The entorhinal cortex projections to the dentate gyrus and the hippocampus also exhibit clear patterns of laminar and topographical organization, which suggest distinct functional circuits (Amaral, Kondo, & Lavenex, 2014; Witter et al., 1989; Witter & Amaral, 1991). Entorhinal cortex projections to the dentate gyrus, CA3, and CA2 originate mainly from Layer II neurons, and to a much lesser extent from Layer VI neurons. In contrast, projections to CA1 and the subiculum originate mainly from Layer III neurons, and to a much lesser extent from Layer V neurons. The dentate gyrus and CA3 do not project back to the entorhinal cortex (Amaral & Lavenex, 2007; Lavenex & Amaral, 2000). In contrast, CA1 and the subiculum project to the deep layers of the entorhinal cortex, following a topographical organization that reciprocates the entorhinal cortex projections to these regions (Amaral & Lavenex, 2007; Lavenex & Amaral, 2000). Another characteristic of the connectivity of the entorhinal cortex is the direct projection from the presubiculum to Layer III of the caudal entorhinal cortex areas Ec and Ecl. In contrast, projections from the parasubiculum terminate in Layer II in all subdivisions of the entorhinal cortex, although the projections to the rostral subdivisions may be less robust (Amaral & Lavenex, 2007). Interestingly, normative data on the volume, neuron number and neuronal soma size in the different layers of the seven subdivisions of the adult rhesus monkey entorhinal cortex (Piguet et al., 2018) corroborated the structural differences in connectivity and histochemical patterns previously described (Amaral et al., 1987). In addition, differences in the number of neurons contributing to distinct afferent and efferent hippocampal pathways suggest that the nature of the interactions between the entorhinal cortex and the rest of the hippocampal formation may vary between subdivisions (Piguet et al., 2018).

1.2 | Development of the entorhinal cortex

Although the entorhinal cortex has been the subject of numerous functional studies, particularly in rodents, there has been no systematic investigation of its postnatal structural development that includes its different layers and subdivisions in either rats, monkeys, or humans. In humans, the overall cytoarchitectonic organization of the entorhinal cortex is clearly identifiable at birth (Grateron et al., 2003). However, although the expression of several calcium-binding proteins is detected in the newborn entorhinal cortex, qualitative observations

suggested that some modifications occur postnatally. For example, calbindin-positive neurons are found almost exclusively in the superficial Layers II and III at 5 months of age, whereas calbindin-positive neurons are also found in Layers V and VI in adulthood. Similarly, no parvalbumin-positive neurons are detected at birth, but they are clearly visible and most abundant at lateral and caudal levels of the entorhinal cortex by 5 months of age.

In monkeys, qualitative observations of nonphosphorylated, high-molecular-weight neurofilament immunostaining revealed that the neurons located in Layers II and III of Ei mature earlier than those located in Layers V and VI (Lavenex et al., 2004, 2007). However, in the absence of systematic, quantitative information, it is difficult to extrapolate from these observations to other subdivisions of the primate entorhinal cortex that receive different cortical afferents. Nor is it possible to determine the exact ages at which morphological changes take place that may reflect the structural maturation of different neuronal populations. Such information is particularly relevant in order to determine whether putative functional circuits processing different types of sensory inputs mature simultaneously or at different times during early postnatal life.

1.3 | Aim of the study

This study aimed to provide normative data on the structural development of the seven subdivisions of the rhesus macaque monkey entorhinal cortex during early postnatal life. We implemented stereological techniques to provide estimates of neuron number, neuronal soma size, and volume of the different layers and subdivisions of the entorhinal cortex in male and female monkeys at 1 day, 6 months, 1 year, and 5–9 years of age. Consistent with previous findings in the hippocampal formation (Jabès et al., 2010, 2011), we found that different layers and subdivisions of the entorhinal cortex exhibit different profiles of structural development.

2 | MATERIALS AND METHODS

2.1 | Experimental animals

Sixteen rhesus monkeys, *Macaca mulatta*, four 1-day-olds (2 M, 2 F), four 6-month-olds (2 M, 2 F), four 1-year-olds (2 M, 2 F), and four adults (5.3, 9.4 [M], 7.7 and 9.3 [F] years of age) were used. Monkeys were born from multiparous mothers and raised at the California National Primate Research Center (CNPRC). They were maternally reared in 2,000-m^2 outdoor enclosures and lived in large social groups until they were killed. These animals were part of the same animals used in studies on the postnatal development of the hippocampal formation (Jabès et al., 2010, 2011) and amygdala (Chareyron, Banta Lavenex, Amaral, & Lavenex, 2011, 2012). All experimental procedures were approved by the Institutional Animal Care and Use Committee of the University of California, Davis, and were in accordance with the National Institutes of Health guidelines for the use of animals in research.

2.2 | Histological processing

2.2.1 | Brain acquisition

Monkeys were deeply anesthetized with an intravenous injection of sodium pentobarbital (50 mg/kg i.v.; FatalPlus; Vortech Pharmaceuticals, Dearborn, MI) and perfused transcardially with 1% and then 4% paraformaldehyde in 0.1 M phosphate buffer (PB; pH 7.4) following standard protocols (Lavenex, Banta Lavenex, Bennett, & Amaral, 2009). Coronal sections were cut with a freezing, sliding microtome in six series at 30-μm, and one series at 60-μm (Microm HM 450; Microm Int. GmbH, Walldorf, Germany). The 60-μm sections were collected in 10% formaldehyde solution in 0.1 M PB (pH 7.4) and post-fixed at 4°C for 4 weeks prior to Nissl staining with thionin. All other series were collected in tissue collection solution (TCS) and kept at −70°C until further processing.

2.2.2 | Nissl staining

The procedure for Nissl-stained sections followed standard protocols (Lavenex et al., 2009). Sections were removed from 10% formaldehyde solution, thoroughly washed for 2 × 2 hr in 0.1 M PB (pH 7.4), mounted on gelatin-coated slides from filtered 0.05 M phosphate buffer (pH 7.4), and air-dried overnight at 37°C. Sections were then defatted for 2 × 2 hr in a mixture of chloroform/ethanol (1:1, vol.) and rinsed for 2 × 2 min in 100% ethanol, 1× 2 min in 95% ethanol, and air-dried overnight at 37°C. Sections were then rehydrated through a graded series of ethanol, 2 min in 95% ethanol, 2 min in 70% ethanol, 2 min in 50% ethanol; dipped in two separate baths of dH_2O; and stained for 20 s in a 0.25% thionin solution (Fisher Scientific, Waltham, MA; catalog No. T-409), then dipped in two separate baths of dH_2O, 4 min in 50% ethanol, 4 min in 70% ethanol, 4 min in 95% ethanol + glacial acetic acid (1 drop per 100 ml of ethanol), 4 min in 95% ethanol, 2 × 4 min in 100% ethanol, 3 × 4 min in xylene; and coverslipped with DPX (BDH Laboratories, Poole, United Kingdom).

2.3 | Stereological analyses

2.3.1 | Structural organization of the monkey entorhinal cortex

The nomenclature, topographical, and cytoarchitectonic organization of the entorhinal cortex were initially described for the cynomolgus monkey (*Macaca fascicularis*; Amaral et al., 1987). The monkey entorhinal cortex comprises seven subdivisions (Figures 1 and 2). Although the cytoarchitectonic characteristics of the cynomolgus monkey and rhesus monkey (*Macaca mulatta*) entorhinal cortex are very similar, there are subtle species differences in the relative development of individual layers in certain subdivisions. We previously described the cytoarchitectonic characteristics of the adult rhesus monkey entorhinal cortex (Piguet et al., 2018). Here, we followed the same

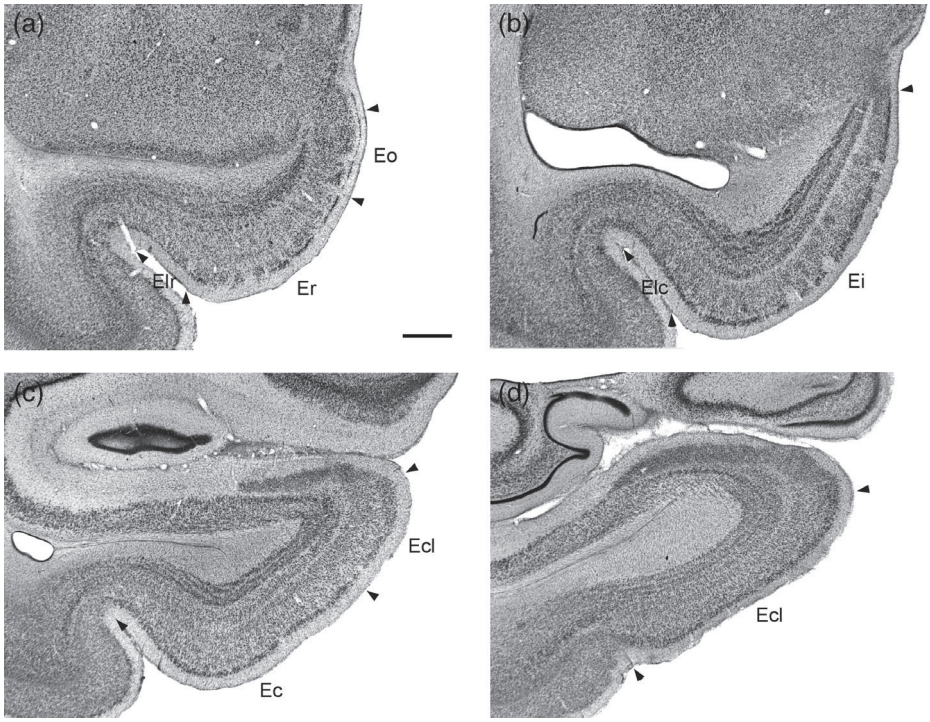

FIGURE 1 Low magnification photomicrographs of coronal sections through the adult rhesus monkey entorhinal cortex. Nissl-stained preparations, arranged from rostral (a) to caudal (d). Eo, olfactory subdivision; Er, rostral subdivision; Elr, lateral rostral subdivision; Elc, lateral caudal subdivision; Ei, intermediate subdivision; Ec, caudal subdivision; Ecl, caudal limiting subdivision. Scale bar = 1 mm

cytoarchitectonic criteria to perform a stereological analysis of the postnatal structural development of the entorhinal cortex.

2.3.2 | Neuron number

The total number of neurons in the different layers of the seven subdivisions of the monkey entorhinal cortex was determined using the optical fractionator method on 60-μm Nissl-stained sections (West, Slomianka, & Gundersen, 1991). For 1-day-old and adult monkeys, about 38 sections per animal (240 μm apart) were used, with the first section selected randomly within the first two sections of Eo. For 6-month-old and 1-year-old monkeys, about 17 sections per animal (480 μm apart) were used. We used a 100X Plan Fluor oil objective (N.A. 1.30) on a Nikon Eclipse 80i microscope (Nikon Instruments Inc, Melville, NY) linked to PC-based StereoInvestigator 9.0 (MicroBrightField, Williston, VT). See Piguet et al. (2018) for other parameters.

2.3.3 | Neuronal soma size

Neuronal soma size was determined using the nucleator method (Gundersen, 1988). We measured an average of 200 neurons per layer per subdivision, sampled at every counting site during the optical fractionator analysis. The nucleator can be used to estimate the mean volume of cells. A set of rays emanating from a randomly chosen point within the nucleus or nucleolus is drawn and oriented randomly. The length of the intercept from the point to the cell boundary (l) is measured, and the cell volume is obtained by $V = (4/3*3.1416)*l^3$.

2.3.4 | Volume of individual layers in distinct subdivisions

We estimated the volume of the individual layers of the seven subdivisions of the monkey entorhinal cortex based on the outline tracings performed for the estimation of neuron numbers. We used the section cutting thickness (60 μm) to determine the distance between sampled sections, which was then multiplied by the total surface area to calculate the volume of individual layers.

2.4 | Statistical analyses

We performed general linear model (GLM) analyses with age as a factor, and regions and layers as repeated measures, to compare the postnatal development of distinct entorhinal subdivisions or layers. We performed GLM analyses with age as a factor to analyze volume, neuronal soma size, and neuron number within individual layers of each subdivision. Degrees of freedom were adjusted following the Greenhouse–Geisser method, when the Mauchly's test of sphericity for repeated measures was significant. We report effect size with η^2_p (partial eta squared, as reported by SPSS 25.0, IBM statistics). We performed post hoc analyses with the Fisher-LSD test when the *F* ratio was significant, thus controlling for Type I error rate (Carmer & Swanson, 1973). Significance level was set at a two-tailed p value < .05 for GLM analyses and post hoc tests, unless specified otherwise for some comparisons between individual age groups (listed two-tailed p value < .10, which corresponds to a one-tailed p value < .05). All statistical analyses were performed on absolute values. Percentages of adult values are reported on figures and in

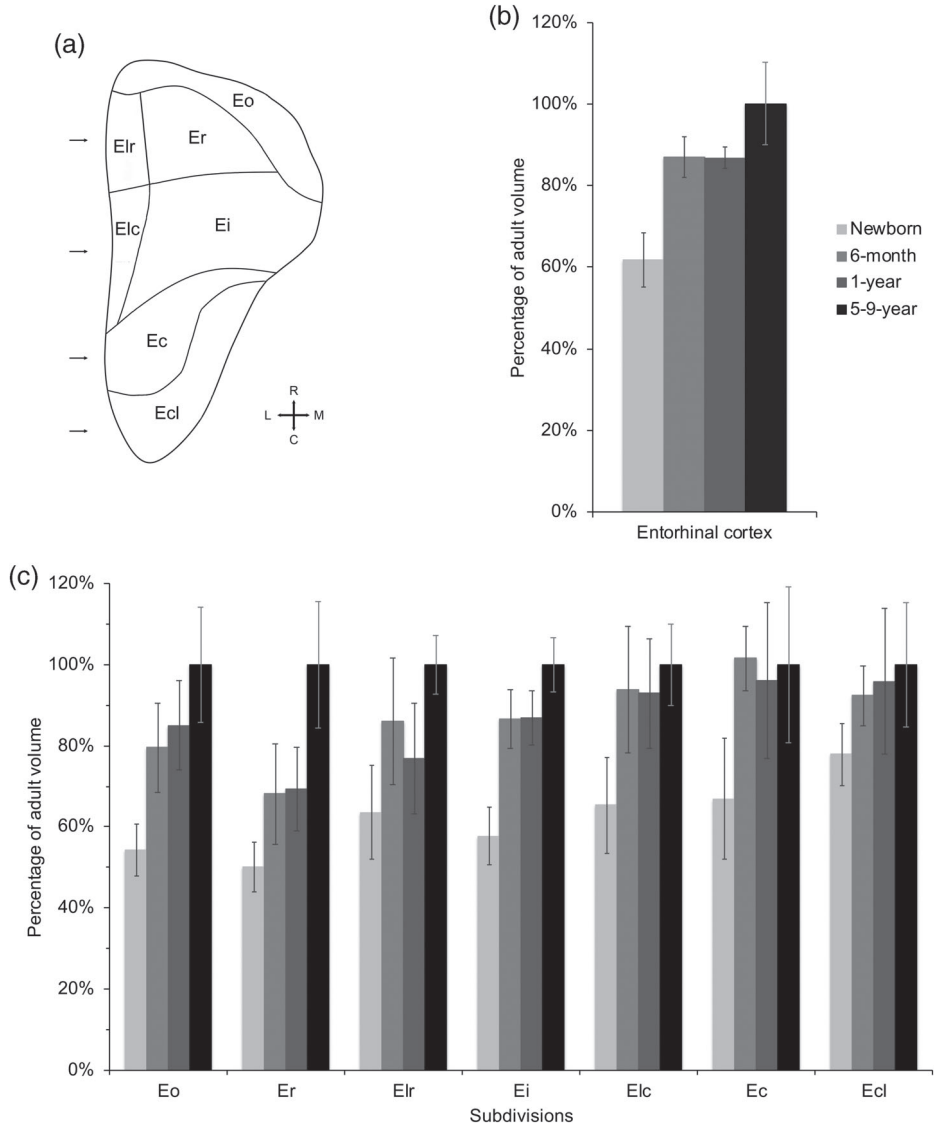

FIGURE 2 (a) Unfolded map of the rhesus monkey entorhinal cortex illustrating the relative position of its seven subdivisions. Black arrows indicate the approximate rostrocaudal locations of the coronal sections illustrated in Figure 1. (b) Percentage of the adult volume of the entire entorhinal cortex, at different ages during postnatal development. (c) Percentage of the adult volumes of the seven subdvisions of the entorhinal cortex, at different ages during postnatal development. See main text for details

the text to facilitate the comparisons of different developmental patterns.

No consistent sex differences were found for the measured parameters, so data from both sexes were combined for presentation. We also evaluated each structure in a systematic manner on the left or right side of the brain: we measured the left entorhinal cortex for one male and one female, and the right entorhinal cortex for one male and one female, in each age group. No lateralization was found for any of the measured parameters.

2.5 | Photomicrographic production

Photomicrographs were taken with a Leica DFC420 digital camera on a Leica MZ9.5 stereomicroscope (Leica Microsystems GmbH, Wetzlar, Germany). Artifacts located outside the sections were removed and levels were adjusted in Adobe Photoshop CS4 V11.0.2 (Adobe Systems, San Jose, CA) to improve contrast.

3 | RESULTS

3.1 | Volume

3.1.1 | Volume of different subdivisions

We first compared age-related changes in volume of the seven subdivisions of the monkey entorhinal cortex during early postnatal development (Figure 2; Tables 1 and 2). As expected, there were differences in the volume of the different subdivisions averaged across all ages ($F_{(6,72)}$ = 259.001, p < .001, η^2_p = .956; Elr (7% of entire entorhinal cortex volume) = Elc (7%) < Eo (10%) < Er (13%) < Ec (18%) = Ecl (17%) < Ei (28%)), as well as differences between age groups ($F_{(3,12)}$ = 23.016, p < .001, η^2_p = .852). In newborn monkeys, the volume of the entire entorhinal cortex was 62% of the adult volume (p < .001). It increased from birth to 6 months of age (p < .001), when it was 87% of the adult volume (6-month vs. 5–9-year, p = .016). It remained stable between 6 months and 1 year of age

TABLE 1 Average volume (mm^3 ± *SD*) of the different layers of the seven subdivisions of the rhesus monkey entorhinal cortex at four postnatal ages

		Newborn	6-month	1-year	5–9-year
Eo	I	0.88 ± 0.19	1.10 ± 0.06	1.08 ± 0.13	0.86 ± 0.25
	II	0.74 ± 0.13	0.96 ± 0.12	0.99 ± 0.16	0.98 ± 0.17
	III	3.68 ± 0.51	5.63 ± 0.94	6.33 ± 0.77	7.78 ± 1.31
	V–VI	0.98 ± 0.12	1.53 ± 0.22	1.45 ± 0.39	1.97 ± 0.28
	Eo total	**6.28 ± 0.74**	**9.22 ± 1.29**	**9.86 ± 1.28**	**11.59 ± 1.66**
Er	I	1,23 ± 0,28	1,52 ± 0,38	1,37 ± 0,26	1,50 ± 0,39
	II	0.87 ± 0.16	1.30 ± 0.27	1.28 ± 0.24	1.47 ± 0.28
	III	3.71 ± 0.44	5.01 ± 0.83	5.65 ± 0.92	8.24 ± 1.26
	V	0.82 ± 0.12	1.11 ± 0.22	1.04 ± 0.11	1.83 ± 0.40
	VI	1.50 ± 0.25	2.13 ± 0.42	1.89 ± 0.24	3.20 ± 0.55
	Er total	**8.13 ± 1.01**	**11.06 ± 2.01**	**11.24 ± 1.67**	**16.24 ± 2.54**
Elr	I	0.81 ± 0.14	1.08 ± 0.40	0.87 ± 0.20	1.08 ± 0.08
	II	0.52 ± 0.08	0.77 ± 0.13	0.68 ± 0.08	0.88 ± 0.16
	III	1.50 ± 0.27	1.96 ± 0.43	1.88 ± 0.31	2.42 ± 0.17
	V	0.63 ± 0.12	0.86 ± 0.05	0.74 ± 0.04	1.08 ± 0.09
	VI	1.14 ± 0.24	1.57 ± 0.23	1.39 ± 0.11	1.78 ± 0.09
	Elr total	**4.60 ± 0.84**	**6.23 ± 1.17**	**5.56 ± 0.60**	**7.24 ± 0.53**
Ei	I	2.88 ± 0.42	4.04 ± 0.53	3.79 ± 0.42	4.37 ± 0.56
	II	1.95 ± 0.22	3.31 ± 0.44	3.20 ± 0.36	3.56 ± 0.25
	III	7.11 ± 1.07	9.66 ± 0.86	10.17 ± 0.63	11.16 ± 0.57
	IV	0.52 ± 0.14	0.69 ± 0.09	0.74 ± 0.09	1.25 ± 0.23
	V	2.18 ± 0.27	3.30 ± 0.50	2.95 ± 0.30	3.92 ± 0.50
	VI	2.72 ± 0.29	5.05 ± 0.36	5.32 ± 0.83	5.82 ± 0.99
	Ei total	**17.35 ± 2.15**	**26.04 ± 2.18**	**26.17 ± 2.01**	**30.08 ± 1.99**
Elc	I	0.88 ± 0.16	1.20 ± 0.20	1.18 ± 0.03	1.25 ± 0.23
	II	0.45 ± 0.07	0.76 ± 0.14	0.75 ± 0.11	0.89 ± 0.07
	III	1.55 ± 0.32	1.81 ± 0.37	1.96 ± 0.39	2.27 ± 0.26
	V	0.62 ± 0.17	0.92 ± 0.21	0.85 ± 0.17	0.96 ± 0.14
	VI	1.00 ± 0.19	1.77 ± 0.27	1.66 ± 0.25	1.52 ± 0.19
	Elc total	**4.50 ± 0.82**	**6.47 ± 1.07**	**6.40 ± 0.94**	**6.89 ± 0.70**
Ec	I	2.01 ± 0.44	2.83 ± 0.43	2.66 ± 0.40	2.75 ± 0.58
	II	1.21 ± 0.20	2.13 ± 0.04	2.01 ± 0.46	2.18 ± 0.36
	III	4.89 ± 1.26	6.71 ± 0.46	6.44 ± 1.33	6.61 ± 1.44
	V	1.48 ± 0.33	2.51 ± 0.20	2.21 ± 0.71	2.75 ± 0.53
	VI	2.43 ± 0.55	4.09 ± 0.54	3.95 ± 0.88	3.68 ± 0.81
	Ec total	**12.03 ± 2.68**	**18.27 ± 1.43**	**17.26 ± 3.47**	**17.98 ± 3.46**
Ecl	I	2.71 ± 0.23	3.25 ± 0.45	3.13 ± 0.71	3.13 ± 0.28
	II	1.91 ± 0.22	2.53 ± 0.21	2.64 ± 0.41	2.83 ± 0.44
	III	5.24 ± 0.75	6.08 ± 0.39	6.47 ± 1.32	6.19 ± 1.03
	V	1.26 ± 0.07	1.49 ± 0.11	1.54 ± 0.32	2.01 ± 0.34
	VI	2.06 ± 0.26	2.27 ± 0.29	2.43 ± 0.42	2.76 ± 0.59
	Ecl total	**13.17 ± 1.29**	**15.62 ± 1.27**	**16.22 ± 3.03**	**16.91 ± 2.58**
Entire EC		**66.06 ± 7.07**	**92.90 ± 5.38**	**92.71 ± 2.77**	**106.92 ± 10.77**

(p = .971), at 87% of the adult volume. It differed between 1 year and 5–9 years of age (p = .015). However, we also found an interaction between subdivisions and age groups ($F_{(18,72)}$ = 4.047, p < .001, η^2_p = .503), which indicated different profiles of postnatal volumetric changes in the different subdivisions of the monkey entorhinal cortex (Figure 2c).

Based on analyses presented below, we defined several developmental profiles: (a) *Very early maturation*: newborn = 6-month = 1-year = 5–9-year.

TABLE 2 Results of the statistical analyses on the volume (mm^3 ± *SD*) of the different layers of the seven subdivisions of the rhesus monkey entorhinal cortex at four postnatal ages

		Profile	$F_{(3,12)}$	*p*	η^2_p	Post hoc comparisons
Eo	I	Very early	2.240	.136	.359	None significant
	II	Early	2.611	.100	.395	Newborn < 6-month — 1-year — 5–9-year
	III	Two-step	13.460	.000	.771	Newborn < 6-month — 1-year < 5–9-year
	V-VI	Two-step	9.159	.002	.696	Newborn < 6-month — 1-year < 5–9-year
	Eo total	**Two-step**	**11.825**	**.001**	**.747**	**Newborn < 6-month — 1-year < 5–9-year**
Er	I	Very early	0.677	.583	.145	None significant
	II	Early	4.365	.027	.522	Newborn < 6-month — 1-year — 5–9-year
	III	Two-step/late	17.476	.000	.814	Newborn < 6-month — 1-year < 5–9-year
	V	Late	12.753	.000	.761	Newborn — 6-month — 1-year < 5–9-year
	VI	Two-step/late	14.301	.000	.781	Newborn < 6-month — 1-year < 5–9-year
	Er total	**Two-step/late**	**12.635**	**.001**	**.760**	**Newborn < 6-month — 1-year < 5–9-year**
Elr	I	Very early	1.467	.273	.268	None significant
	II	Two-step	6.383	.008	.615	Newborn < 6-month — 1-year < 5–9-year
	III	Two-step	5.883	.010	.595	Newborn < 6-month — 1-year < 5–9-year
	V	Two-step	21.879	.000	.845	Newborn < 6-month — 1-year < 5–9-year
	VI	Two-step	8.918	.002	.690	Newborn < 6-month — 1-year < 5–9-year
	Elr total	**Two-step**	**7.226**	**.005**	**.644**	**Newborn < 6-month — 1-year < 5–9-year**
Ei	I	Early	6.920	.006	.634	Newborn < 6-month — 1-year — 5–9-year
	II	Early	19.265	.000	.828	Newborn < 6-month — 1-year — 5–9-year
	III	Two-step/early	18.384	.000	.821	Newborn < other ages; 6-month < 5–9-year
	IV	Late	18.088	.000	.819	Newborn — 6-month — 1-year < 5–9-years
	V	Two-step	12.702	.000	.761	Newborn < 6-month — 1-year < 5–9-year
	VI	Early	16.188	.000	.802	Newborn < 6-month — 1-year — 5–9-year
	Ei total	**Two-step/early**	**26.645**	**.000**	**.869**	**Newborn < 6-month — 1-year < 5–9-year**
Elc	I	Early	3.804	.040	.487	Newborn < 6-month — 1-year — 5–9-year
	II	Two-step/early	14.482	.000	.784	Newborn < 6-month — 1-year < 5–9-year
	III	Gradual	3.156	.064	.441	Newborn < 5–9-year
	V	Early	3.003	.073	.429	Newborn < 6-month — 1-year — 5–9-year
	VI	Early	8.871	.002	.689	Newborn < 6-month — 1-year — 5–9-year
	Elc total	**Early**	**5.686**	**.012**	**.587**	**Newborn < 6-month — 1-year — 5–9-year**
Ec	I	Early	2.562	.104	.390	Newborn < 6-month — 1-year — 5–9-year
	II	Early	8.498	.003	.680	Newborn < 6-month — 1-year — 5–9-year
	III	Early	2.065	.158	.341	Newborn < 6-month — 1-year — 5–9-year
	V	Early	5.193	.016	.565	Newborn < 6-month — 1-year — 5–9-year
	VI	Early	4.544	.024	.532	Newborn < 6-month — 1-year — 5–9-year
	Ec total	**Early**	**4.150**	**.031**	**.509**	**Newborn < 6-month — 1-year — 5–9-year**
Ecl	I	Very early	1.103	.386	.216	None significant
	II	Early	5.656	.012	.586	Newborn < 6-month — 1-year — 5–9-year
	III	Very early	1.275	.327	.242	None significant
	V	Early - late	6.641	.007	.624	Newborn — 6-month — 1-year < 5–9-year
	VI	Early - gradual	2.066	.158	341	Newborn < 5–9-year
	Ecl total	**Early**	**2.214**	**.139**	**.356**	**Newborn < 1-year — 5–9-year**
Entire EC		**Two-step/early**	**23.016**	**.000**	**.852**	**Newborn < 6-month — 1-year < 5–9-year**

(b) *Early maturation*: newborn < 6-month = 1-year = 5–9-year. We also considered the percentage of the adult volume at specific ages in order to further characterize this developmental profile, because a particular structure may be volumetrically more developed than another structure at birth but show later volumetric changes during postnatal development: *Early — Late*: newborn — 6-month — 1-year < 5–9-year; *Early — Gradual*: newborn < 5–9-year. (c) *Two-step maturation*: newborn < 6-month = 1-year < 5–9-year. This profile was further characterized as a *Two-step/early* profile when the volume at 6 months and 1 year of age was higher than 85% of the adult volume, and a *Two-step/late* profile when the volume at 6 months and 1 year of age was lower than 70% of the adult volume. (d) *Gradual maturation*: newborn < 6-month < 1-year < 5–9-year. (e) *Late maturation*: newborn = 6-month = 1-year < 5–9-year.

Eo exhibited a two-step maturation profile. It was 54% of the adult volume at birth ($p < .001$), and increased to 80% at 6 months of age (newborn vs. 6-month: $p = .007$). There was no difference in the volume of Eo between 6-month-old and 1-year-old monkeys (85%; $p = .495$), whereas it differed between 1-year-old and 5–9-year-old monkeys ($p = .081$).

Er exhibited a two-step/late maturation profile. It was 50% of the adult volume at birth ($p < .001$), and increased to 68% at 6 months of age (newborn vs. 6-month: $p = .049$). There was no difference in the volume of Er between 6-month-old and 1-year-old monkeys (69%; $p = .897$), whereas it differed between 1-year-old and 5–9-year-old monkeys ($p = .003$).

Elr exhibited a two-step maturation profile. It was 64% of the adult volume at birth ($p = .001$), and increased to 86% at 6 months of age (newborn vs. 6-month: $p = .016$). There was no difference in the volume of Elr between 6-month-old and 1-year-old monkeys (77%; $p = .276$), whereas it differed between 1-year-old and 5–9-year-old monkeys ($p = .014$).

Ei exhibited a two-step/early maturation profile. It was 58% of the adult volume at birth ($p < .001$), and increased to 87% at 6 months of age (newborn vs. 6-month: $p < .001$). There was no difference in the volume of Ei between 6-month-old and 1-year-old monkeys (87%; $p = .929$), whereas it differed between 1-year-old and 5–9-year-old monkeys ($p = .021$).

Elc exhibited an early maturation profile. It was 65% of the adult volume at birth ($p = .003$), and increased to 94% at 6 months of age (newborn vs. 6-month: $p = .009$). There was no difference in the volume of Elc between 6-month-old and 1-year-old monkeys (93%; $p = .916$), or between 1-year-old and 5–9-year-old monkeys ($p = .453$).

Ec exhibited an early maturation profile. It was 67% of the adult volume at birth ($p = .013$), and increased to 102% at 6 months of age (newborn vs. 6-month: $p = .010$). There was no difference in the volume of Ec between 6-month-old and 1-year-old monkeys (96%; $p = .631$), or between 1-year-old and 5–9-year-old monkeys ($p = .732$).

Ecl exhibited an early to very early maturation profile. It was 78% of the adult volume at birth ($p = .032$), and, although it increased to 92% at 6 months of age, the difference between newborn and 6-month-old monkeys was not statistically significant ($p = .139$). There was no difference in the volume of Ecl between 6-month-old and 1-year-old monkeys (96%; $p = .705$), or between 1-year-old and 5–9-year-old monkeys ($p = .663$).

In sum, the seven subdivisions of the monkey entorhinal cortex exhibited different profiles of volumetric changes during early postnatal life: Er exhibited a two-step/late maturation profile; Eo and Elr exhibited a two-step maturation profile; Ei exhibited a two-step/early maturation profile; Elc, Ec, and Ecl exhibited an early maturation profile.

3.1.2 | Volume of the distinct layers of different subdivisions

Following the characterization of different profiles of postnatal volumetric development of the different subdivisions of the monkey entorhinal cortex, we analyzed the profiles of postnatal volumetric development of distinct layers within each subdivision (Figure 3; Tables 1 and 2).

Global analysis

We first performed a global GLM analysis with repeated measures on the five layers (I, II, III, V, VI) that are common to six subdivisions (Er, Ei, Elr, Elc, Ec, Ecl), thus excluding all layers of Eo and Layer IV of Ei for this analysis. We found differences between age groups ($F_{(3,12)} = 22.296$, $p < .001$, $\eta^2_p = .848$), subdivisions ($F_{(5,60)} = 243.913$, $p < .001$, $\eta^2_p = .953$) and layers ($F_{(4,48)} = 959.934$, $p < .001$, $\eta^2_p = .988$), as well as significant interactions between age groups and subdivisions ($F_{(15,60)} = 3.928$, $p < .001$, $\eta^2_p = .495$), age groups and layers ($F_{(12,48)} = 7.791$, $p < .001$, $\eta^2_p = .661$), subdivisions and layers ($F_{(20,240)} = 146.224$, $p < .001$, $\eta^2_p = .924$), and age groups, subdivisions and layers ($F_{(60,240)} = 4.408$, $p < .001$, $\eta^2_p = .524$). This global analysis demonstrated that distinct layers of different subdivisions of the monkey entorhinal cortex exhibited different profiles of postnatal volumetric development. Based on these results, we performed two series of additional analyses. First, we compared the volumetric development of each layer across all subdivisions. Second, we compared the volumetric development of all layers within each subdivision. Although some information presented below is partly redundant, these two series of analyses are justified in order to provide comprehensive comparisons of the developmental profiles of individual layers both within and across individual subdivisions.

Analyses per layer across subdivisions

Layer I exhibited different postnatal volumetric maturation profiles in different subdivisions: age groups ($F_{(3,12)} = 4.611$, $p = .023$, $\eta^2_p = .535$; newborn < 6-month — 1-year — 5–9-year), subdivisions ($F_{(3.578,42.931)} = 234.792$, $p < .001$, $\eta^2_p = .951$), interaction ($F_{(10.733,42.931)} = 2.101$, $p = .042$, $\eta^2_p = .344$). There were no statistically significant overall differences between age groups in the volume of Layer I in Eo, Er, Elr, Ec, and Ecl. In contrast, there were differences between age groups in the volume of Layer I in Ei and Elc. Despite subtle differences between subdivisions, the postnatal volumetric

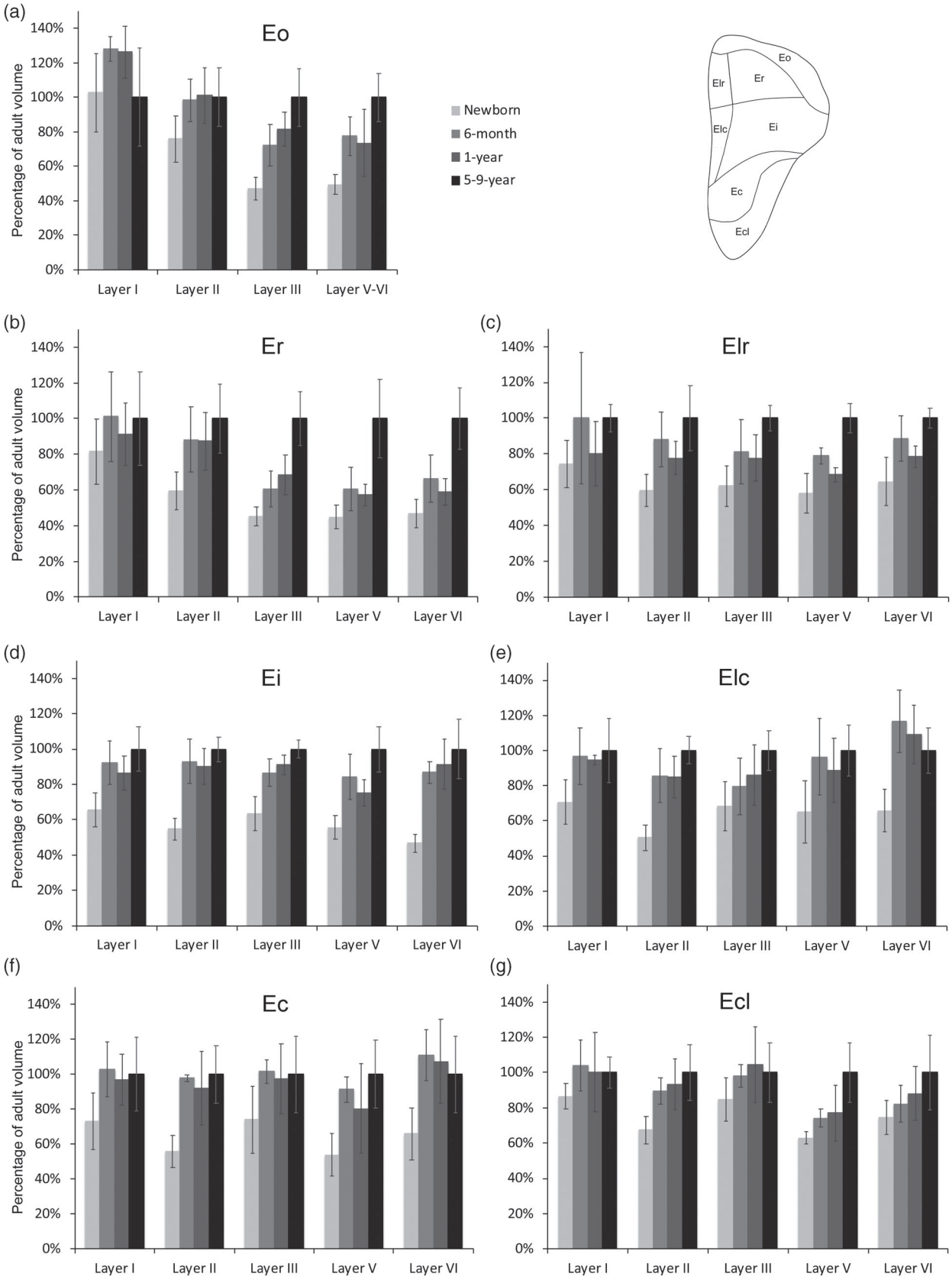

FIGURE 3 Percentage of the adult volume of the different layers of the seven subdivisions of the monkey entorhinal cortex, at different ages during postnatal development. (a) Area Eo; (b) area Er; (c) area Elr; (d) area Ei; (e) area Elc; (f) area Ec; (g) area Ecl. See main text for details

development of Layer I exhibited an early to very early maturation profile (>92% of adult volume at 6 months of age) in all subdivisions.

Layer II exhibited different postnatal volumetric maturation profiles in different subdivisions: age groups ($F_{(3,12)}$ = 19.183, p < .001, η^2_p = .827; newborn < 6-months — 1-year — 5–9-years), subdivisions ($F_{(2.988,35.856)}$ = 296.197, p < .001, η^2_p = .961), interaction ($F_{(8.964,35.856)}$ = 4.348, p = .001, η^2_p = .521). Despite the fact that in Eo the volume of Layer II was 76% of the adult volume in newborn monkeys (p = .041), the overall difference between age groups failed to reach statistical significance. In contrast, there were differences between age groups in the volume of Layer II in Er, Elr, Ei, Elc, Ec, and Ecl. Accordingly, and despite minor peculiarities in Elr (two-step profile) and Elc (two-step/early profile), the postnatal volumetric development of Layer II exhibited an early maturation profile in most subdivisions.

Layer III exhibited different postnatal volumetric maturation profiles in different subdivisions: age groups ($F_{(3,12)}$ = 19.966, p < .001, η^2_p = .833; newborn < 6-month — 1-year < 5–9-year), subdivisions ($F_{(6,72)}$ = 197.902, p < .001, η^2_p = .943), interaction ($F_{(18,72)}$ = 4.264, p < .001, η^2_p = .516). There were differences between age groups in the volume of Layer III in Eo, Er, Elr, and Ei. In both Elc and Ec, although the volume of Layer III was less than 75% of the adult volume in newborns, the overall difference between age groups failed to reach statistical significance. There were no differences between age groups in the volume of Layer III in Ecl. Accordingly, the postnatal volumetric development of Layer III exhibited a clear rostro-caudal gradient, with a two-step/late maturation profile in Er, a two-step maturation profile in Eo and Elr, a gradual maturation profile in Elc, a two-step/early maturation profile in Ei, and an early to very early maturation profile in Ec and Ecl.

Layer IV is only present in Ei. There were differences between age groups in the volume of Layer IV. It was 42% of the adult volume at birth, 55% at 6 months and 59% at 1 year of age; it was larger in adults compared to all other ages (all p < .001). Accordingly, Layer IV of Ei exhibited a late maturation profile.

Layer V exhibited different postnatal volumetric maturation profiles in different subdivisions: age groups ($F_{(3,12)}$ = 29.239, p < .001, η^2_p = .880; newborn < 6-month — 1-year < 5–9-year), subdivisions ($F_{(2.861,34.336)}$ = 130.764, p < .001, η^2_p = .916), interaction ($F_{(8.584,34.336)}$ = 2.495, p = .003, η^2_p = .384; note that we considered Layers V–VI of Eo as a Layer V in order to perform this analysis). There were differences between age groups in the volume of Layers V–VI in Eo. Similarly, there were differences between age groups in the volume of Layer V in Er, Elr, Ei, Ec, and Ecl. In Elc, although the volume of Layer V was only 65% of the adult volume in newborns (p = .018), the overall difference between age groups failed to reach statistical significance. Interestingly, the postnatal volumetric development of Layer V exhibited differences between subdivisions, but these differences did not follow a clear rostro-caudal gradient. Layer V exhibited a two-step maturation profile in Eo, Ei, and Elr, a late maturation profile in Er, and an early maturation profile in Elc and Ec. Interestingly, the volume of layer V was as developed in Ecl (63% of adult volume) as in Elc (65%) at birth, but it exhibited a more gradual/late maturation profile to reach adult volume in Ecl.

Layer VI exhibited different postnatal volumetric maturation profiles in different subdivisions: age groups ($F_{(3,12)}$ = 22.588, p < .001, η^2_p = .850; newborn < 6-month — 1-year < 5–9-year), subdivisions ($F_{(3.037,36.439)}$ = 137.275, p < .001, η^2_p = .920), interaction ($F_{(9.110,36.439)}$ = 5.051, p < .001, η^2_p = .558; note that we considered Layers V–VI of Eo as a Layer VI in order to perform this analysis). There were differences between age groups in the volume of Layer VI in Er, Elr, Ei, Elc, and Ec. In Ecl, the volume of Layer VI was 75% of the adult volume in newborn monkeys (p = .033), but the overall difference between age groups was not statistically significant. The postnatal volumetric development of layer VI exhibited a rostro-caudal gradient, with a two-step/late maturation profile in Er, a two-step maturation profile in Elr, an early maturation profile in Ei, Elc, and Ec. In Ecl, the volume of Layer VI was already 75% of the adult volume at birth, but it exhibited a gradual/late maturation profile thereafter, as was observed for Layer V.

Analyses per layer within subdivisions

Eo. The different layers of Eo exhibited different profiles of postnatal volumetric development (Figure 3a): age groups ($F_{(3,12)}$ = 11.825, p = .001, η^2_p = .747; newborn < 6-month — 1-year < 5–9-year), layers ($F_{(1.141,13.691)}$ = 472.975, p < .001, η^2_p = .975), interaction ($F_{(3.423,13.691)}$ = 13.118, p < .001, η^2_p = .766). There were no statistical differences between age groups in the volume of Layer I or II, even though the volume of Layer II was 76% of the adult volume in newborn monkeys (p = .041). In contrast, there were differences between age groups in the volume of Layers III and V–VI. Layers I and II exhibited an early maturation profile, whereas Layers III and V-VI exhibited a two-step maturation profile.

Er. The different layers of Er exhibited different profiles of postnatal volumetric development (Figure 3b): age groups ($F_{(3,12)}$ = 12.635, p = .001, η^2_p = .760; newborn < 6-month — 1-year < 5–9-year), layers ($F_{(1.342,16.110)}$ = 470.038, p < .001, η^2_p = .975), interaction ($F_{(4.027,16.110)}$ = 17.656, p < .001, η^2_p = .815). There was no difference between age groups in the volume of Layer I. In contrast, there were differences between age groups in the volume of Layers II, III, V, and VI. Nevertheless, Layers I and II exhibited an early maturation profile, whereas Layers III, V, and VI exhibited a two-step/late or late maturation profile.

Elr. The different layers of Elr exhibited different profiles of postnatal volumetric development (Figure 3c): age groups ($F_{(3,12)}$ = 7.366, p = .005, η^2_p = .648; newborn < 6-month — 1-year < 5–9-year), layers ($F_{(1.912,22.939)}$ = 233.323, p < .001, η^2_p = .951), interaction ($F_{(5.735,22.939)}$ = 2.682, p = .042, η^2_p = .401). There were no differences between age groups in the volume of Layer I, which exhibited an early maturation profile. In contrast, there were differences between age groups in Layers II, III, V, and VI, which all exhibited a two-step maturation profile.

Ei. The different layers of Ei exhibited different profiles of postnatal volumetric development (Figure 3d): age groups ($F_{(3,12)}$ = 26.645, p < .001, η^2_p = .869; newborn < 6-month — 1-year < 5–9-year), layers ($F_{(2.972,35.661)}$ = 742.411, p < .001, η^2_p = .984), interaction ($F_{(8.915,35.661)}$ = 6.968, p < .001, η^2_p = .635). There were differences

between age groups in all layers. Layers I, II, and VI exhibited an early maturation profile; Layer III exhibited a two-step/early maturation profile; Layer V exhibited a two-step maturation profile; and Layer IV exhibited a late maturation profile.

Elc. The different layers of Elc exhibited different profiles of postnatal volumetric development (Figure 3e): age groups ($F_{(3,12)}$ = 5.686, p = .012, η^2_p = .587; newborn < 6-month — 1-year — 5–9-year), layers ($F_{(4,48)}$ = 193.479, p < .001, η^2_p = .942), interaction ($F_{(12,48)}$ = 3.426, p = .001, η^2_p = .461). Layers I and VI exhibited an early maturation profile. Layer II exhibited a two-step/early maturation profile. The difference between age groups failed to reach statistical significance for the volume of Layers III and V, which exhibited a gradual and early maturation profile, respectively.

Ec. The different layers of Ec exhibited a similar profile of postnatal volumetric development (Figure 3f): age groups ($F_{(3,12)}$ = 4.151, p = .031, η^2_p = .509; newborn < 6-month — 1-year — 5–9-year), layers ($F_{(1.983,23.791)}$ = 236.598, p < .001, η^2_p = .952), interaction ($F_{(5.948,23.791)}$ = 1.138, p = .371, η^2_p = .222). Despite the fact that Layer I was 73% of the adult volume in newborn monkeys (p = .045), the overall difference between age groups was not statistically significant. There were differences between age groups in the volume of Layers II, V, and VI. The difference between age groups in the volume of Layer III did not reach statistical significance, although the maturation profile of Layer III was similar to that of the other layers. Thus, despite some peculiar results for Layers I and III, all layers of Ec exhibited an early maturation profile.

Ecl. Despite the lack of significant interaction between age groups and layers ($F_{(4.663,18.653)}$ = 1.296, p = .308, η^2_p = .245), different layers of Ecl exhibited different profiles of postnatal volumetric development (Figure 3g): age groups ($F_{(3,12)}$ = 2.214, p = .139, η^2_p = .356), layers ($F_{(1.554,18.653)}$ = 390.231, p < .001, η^2_p = .970). There was no difference between age groups in the volume of Layers I and III. There were differences between age groups in the volume of Layers II and V. Although there was no overall difference between age groups in the volume of Layer VI, it was 75% of the adult volume at birth and followed a gradual maturation profile. Thus, the superficial Layers I–III exhibited an early to very early maturation profile. Layer V was already quite large at birth but exhibited a late volumetric expansion to reach adult volume, which we defined as an early–late maturation profile.

3.2 | Neuron number

There were differences in the number of neurons between subdivisions across ages ($F_{(3.317,39.806)}$ = 231.294, p < .001, η^2_p = .951; Elr [6% of all entorhinal cortex neurons] = Elc [6%] < Eo [12%] < Er [12%] < Ec [17%] = Ecl [17%] < Ei [30%]; all p < .001), but no differences between age groups ($F_{(3,12)}$ = 0.799, p = .518, η^2_p = .166; newborn — 6-month — 1-year — 5–9-year), and no interaction between age groups and subdivisions ($F_{(9.952,39.806)}$ = 1.094, p = .390, η^2_p = .215; Table 3).

3.3 | Neuronal soma size

3.3.1 | Global analysis

We first performed a global GLM analysis with repeated measures on the four cellular layers (II, III, V, VI) that are common to six subdivisions (Er, Ei, Elr, Elc, Ec, Ecl), thus excluding area Eo that has only three cellular layers for this analysis. We found differences between age groups ($F_{(3,12)}$ = 17.283, p < .001, η^2_p = .812; newborn < 6-month — 1-year > 5–9-year), subdivisions ($F_{(5,60)}$ = 12.454, p < .001, η^2_p = .509), layers ($F_{(3,36)}$ = 91.197, p < .001, η^2_p = .884), as well as significant interactions between age groups and subdivisions ($F_{(15,60)}$ = 2.618, p = .004, η^2_p = .396), age groups and layers ($F_{(9,36)}$ = 12.559, p < .001, η^2_p = .758), subdivisions and layers ($F_{(15,180)}$ = 23.450 p < .001, η^2_p = .661), and age groups, subdivisions and layers ($F_{(45,180)}$ = 2.325, p < .001, η^2_p = .368). This global analysis demonstrated that the average neuronal soma size exhibited different profiles of postnatal changes in distinct layers of different subdivisions of the monkey entorhinal cortex. Based on these results, we performed two series of additional analyses. First, we compared age-related changes in neuronal soma size within each layer across the seven subdivisions. Second, we compared age-related changes in neuronal soma size across the different layers within each subdivision. Although some information presented below is partly redundant, these two series of analyses are justified in order to provide comprehensive comparisons of the developmental profiles of principal neurons in individual layers both within and across individual subdivisions (Figure 4; Tables 4 and 5).

3.3.2 | Analyses per layer across subdivisions

The developmental profiles of neuronal soma size differed from the developmental profiles of the volume of layers and subdivisions. Based on analyses presented below, we defined several maturation profiles for neuronal soma size: (a) *Late decrease*: newborn = 6-month = 1-year > 5–9-year; (b) *No change*: newborn = 6-month = 1-year = 5–9-year; (c) *Transient*: a transient increase at intermediate ages: newborn < 6-month/1-year > 5–9-year, no difference between newborn and 5–9-year; (d) *Transient increase*: a transient increase at intermediate ages, together with a net increase between birth and adulthood: newborn < 6-month/ 1-year > 5–9-year and newborn < 5–9 year; (e) *Early increase*: newborn < 6-month = 1-year = 5–9-year; (f) *Two-step increase*: newborn < 6-month = 1-year < 5–9-year.

Layer II. The soma size of Layer II neurons exhibited different postnatal developmental profiles in different subdivisions: age groups ($F_{(3,12)}$ = 16.802, p < .001, η^2_p = .808), subdivisions ($F_{(6,72)}$ = 85.734, p < .001, η^2_p = .877), interaction ($F_{(18,72)}$ = 2.440, p = .004, η^2_p = .379). The developmental profile of neuronal soma size exhibited a clear rostro-caudal gradient in Layer II, with a transient increase at 6 months and 1 year of age in Eo, Er, Elr, and Elc, which was followed by a decrease into adulthood; a two-step increase in Ei; and no significant changes in Ec and Ecl.

TABLE 3 Number of neurons in the different layers of the seven subdivisions of the rhesus monkey entorhinal cortex at four postnatal ages

		Newborn	6-month	1-year	5–9-year
Eo	II	56,998 ± 14,616	50,324 ± 11,012	43,573 ± 5,552	40,137 ± 7,108
	III	257,538 ± 53,436	232,567 ± 89,534	239,802 ± 27,701	296,929 ± 41,347
	V-VI	80,202 ± 18,971	91,625 ± 25,452	73,022 ± 13,160	65,969 ± 8,391
	Eo total	**394,738 ± 77,104**	**374,516 ± 121,978**	**356,397 ± 31,283**	**403,035 ± 53,910**
Er	II	49,249 ± 14,977	52,994 ± 15,035	45,477 ± 8,665	50,417 ± 12,078
	III	204,289 ± 55,036	184,467 ± 64,923	188,370 ± 53,426	281,868 ± 48,238
	V	38,259 ± 5,119	34,440 ± 12,002	28,994 ± 5,753	44,363 ± 8,241
	VI	106,700 ± 15,266	110,311 ± 23,743	80,800 ± 4,209	129,493 ± 19,533
	Er total	**398,497 ± 83,570**	**382,212 ± 112,320**	**343,640 ± 68,250**	**506,140 ± 67,352**
Elr	II	32,624 ± 10,586	38,208 ± 10,263	28,238 ± 4,328	37,057 ± 6,695
	III	76,867 ± 22,362	71,202 ± 26,083	67,970 ± 17,254	81,430 ± 8,653
	V	29,578 ± 7,710	30,873 ± 3,640	23,189 ± 4,720	28,949 ± 3,068
	VI	70,389 ± 15,478	67,671 ± 17,161	54,096 ± 5,807	65,686 ± 3,530
	Elr total	**209,458 ± 53,106**	**207,953 ± 54,114**	**173,493 ± 20,000**	**213,123 ± 8,081**
Ei	II	118,911 ± 19,579	130,430 ± 35,204	132,187 ± 33,624	138,243 ± 16,063
	III	388,879 ± 80,299	372,587 ± 51,551	374,793 ± 50,847	445,652 ± 68,989
	V	144,602 ± 25,470	148,560 ± 28,146	104,660 ± 16,160	159,237 ± 20,188
	VI	304,638 ± 52,134	365,010 ± 62,717	299,666 ± 73,535	328,132 ± 46,213
	Ei total	**957,030 ± 161,627**	**1,016,588 ± 130,008**	**911,307 ± 151,217**	**1,071,264 ± 40,889**
Elc	II	26,624 ± 6,395	33,693 ± 6,713	31,826 ± 5,448	38,090 ± 593
	III	70,589 ± 16,528	70,656 ± 18,621	67,518 ± 14,302	83,439 ± 12,414
	V	31,755 ± 7,888	36,877 ± 12,105	28,892 ± 6,343	34,604 ± 3,957
	VI	58,726 ± 9,809	85,161 ± 18,097	70,343 ± 16,279	62,761 ± 7,761
	Elc total	**187,693 ± 38,740**	**226,386 ± 55,094**	**198,579 ± 37,058**	**218,894 ± 22,439**
Ec	II	60,233 ± 21,859	71,250 ± 21,323	75,749 ± 20,533	85,037 ± 13,609
	III	222,020 ± 66,534	214,185 ± 33,337	205,258 ± 54,579	220,281 ± 29,678
	V	80,412 ± 19,808	92,638 ± 20,257	75,549 ± 17,689	88,204 ± 12,656
	VI	174,345 ± 50,666	224,050 ± 47,307	202,147 ± 71,812	185,487 ± 27,211
	Ec total	**537,009 ± 153,077**	**602,124 ± 119,346**	**558,703 ± 151,587**	**579,009 ± 79,525**
Ecl	II	100,238 ± 22,369	99,552 ± 14,937	93,000 ± 14,356	110,802 ± 17,631
	III	260,972 ± 44,181	222,921 ± 37,762	232,836 ± 42,565	211,414 ± 26,276
	V	73,980 ± 12,523	55,641 ± 2,095	56,303 ± 12,150	70,664 ± 8,806
	VI	173,389 ± 33,778	133,312 ± 25,297	145,144 ± 22,267	148,066 ± 18,292
	Ecl total	**608,579 ± 89,027**	**511,427 ± 74,813**	**527,283 ± 70,726**	**540,946 ± 67,937**
Entire EC		**3,293,005 ± 566,029**	**3,321,205 ± 533,323**	**3,069,402 ± 223,207**	**3,532,411 ± 252,997**

Layer III. The soma size of Layer III neurons exhibited different postnatal developmental profiles in different subdivisions: age groups ($F_{(3,12)}$ = 8.837, p = .002, η^2_p = .688), subdivisions ($F_{(3.589,43.068)}$ = 27.854, p < .001, η^2_p = .699), interaction ($F_{(10.767,43.068)}$ = 3.061, p = .004, η^2_p = .434). The developmental profile of neuronal soma size exhibited a clear rostro-caudal gradient in Layer III, with an increase between birth and 6 months of age in Eo, after which soma size remained stable; a transient increase between birth and 6 months of age in Er, Elr, and Ei, which was followed by a gradual decrease into adulthood; and a decrease after 6 months or 1 year of age in Elc, Ec, and Ecl.

Layer V. The soma size of Layer V neurons exhibited different postnatal developmental profiles in different subdivisions: age groups ($F_{(3,12)}$ = 21.891, p < .001, η^2_p = .846), subdivisions ($F_{(6,72)}$ = 25.555, p < .001, η^2_p = .680), interaction ($F_{(18,72)}$ = 2.598, p = .002, η^2_p = .394). The developmental profile of neuronal soma size exhibited a clear rostro-caudal gradient in Layer V. There was an increase between birth and 6 months of age in Eo, after which soma size remained stable; an increase between birth and 6 months of age in all other areas, which was followed by a gradual decrease to reach adult size. Neuronal soma size was smaller in newborn than in 5–9-year-old monkeys

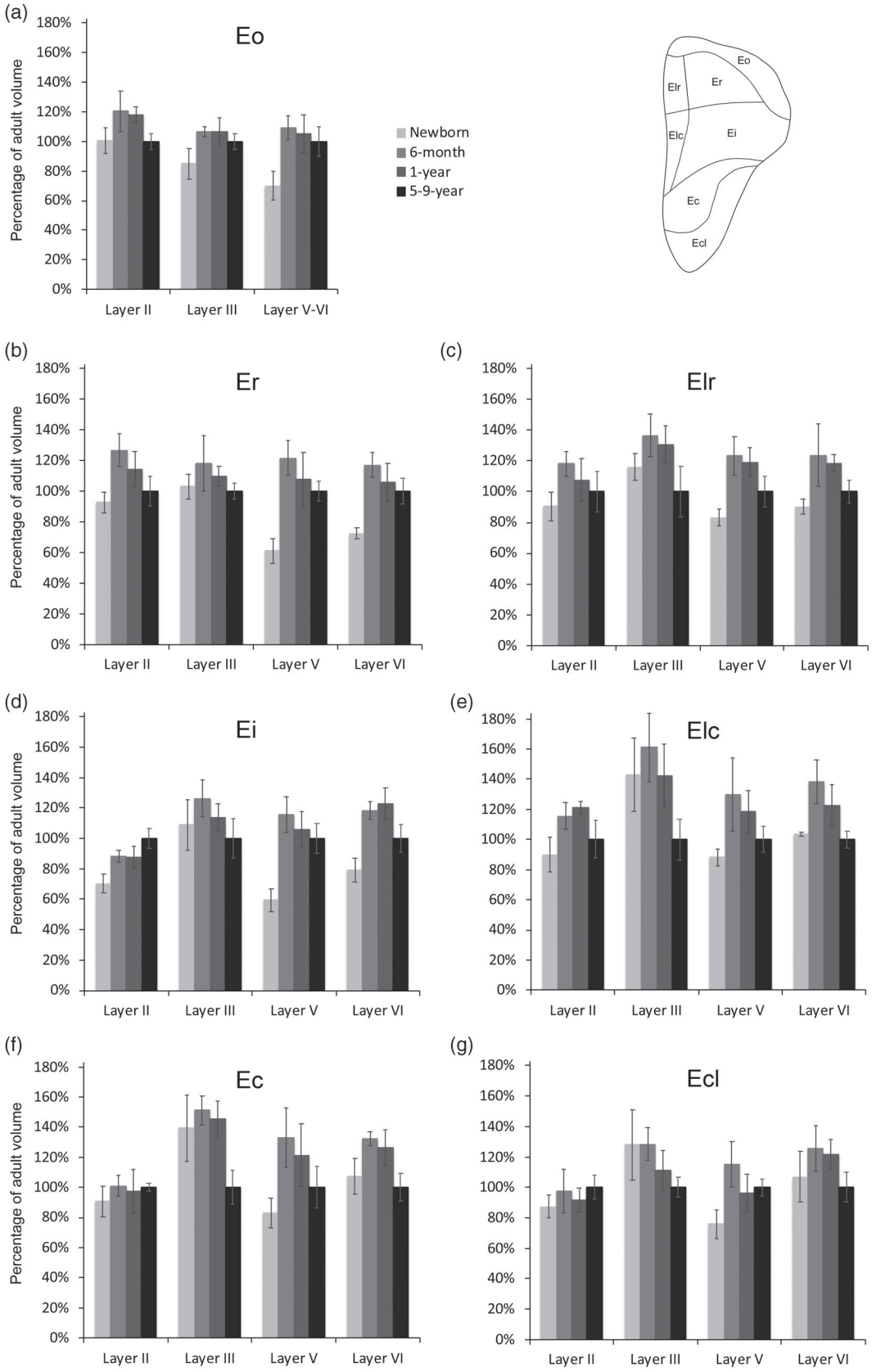

FIGURE 4 Percentage of the adult volume of neuronal soma size in the different layers of the seven subdivisions of the monkey entorhinal cortex, at different ages during postnatal development. (a) Area Eo; (b) area Er; (c) area Elr; (d) area Ei; (e) area Elc; (f) area Ec; and (g) area Ecl. See main text for details

TABLE 4 Neuronal soma size (μm^3 ± *SD*) in the different layers of the seven subdivisions of the rhesus monkey entorhinal cortex at four postnatal ages

		Newborn	6-month	1-year	5–9-year
Eo	II	1,222 ± 107	1,462 ± 169	1,437 ± 65	1,216 ± 66
	III	1,522 ± 183	1,907 ± 62	1,913 ± 171	1,795 ± 95
	V–VI	1,187 ± 168	1,853 ± 135	1,782 ± 213	1,696 ± 171
Er	II	1,509 ± 108	2,064 ± 172	1,858 ± 187	1,629 ± 158
	III	1,904 ± 148	2,187 ± 338	2,027 ± 117	1,850 ± 99
	V	1,444 ± 187	2,877 ± 269	2,552 ± 422	2,370 ± 147
	VI	1,290 ± 62	2,088 ± 149	1,884 ± 218	1,783 ± 152
Elr	II	1,733 ± 178	2,263 ± 152	2,061 ± 270	1,915 ± 254
	III	2,212 ± 166	2,601 ± 264	2,487 ± 234	1,906 ± 316
	V	1,772 ± 115	2,631 ± 266	2,545 ± 203	2,134 ± 219
	VI	1,481 ± 81	2,032 ± 328	1,948 ± 93	1,642 ± 122
Ei	II	1,856 ± 161	2,325 ± 101	2,310 ± 193	2,637 ± 171
	III	2,305 ± 351	2,673 ± 252	2,412 ± 187	2,115 ± 279
	V	1,480 ± 183	2,880 ± 293	2,634 ± 293	2,492 ± 238
	VI	1,385 ± 137	2,075 ± 100	2,151 ± 183	1,755 ± 160
Elc	II	2,049 ± 262	2,632 ± 203	2,765 ± 96	2,280 ± 283
	III	2,456 ± 417	2,773 ± 389	2,446 ± 359	1,721 ± 230
	V	1,844 ± 115	2,712 ± 509	2,473 ± 297	2,089 ± 181
	VI	1,571 ± 24	2,097 ± 219	1,859 ± 211	1,518 ± 87
Ec	II	2,459 ± 279	2,732 ± 187	2,642 ± 394	2,710 ± 67
	III	2,711 ± 428	2,943 ± 185	2,825 ± 240	1,945 ± 218
	V	1,786 ± 213	2,858 ± 422	2,600 ± 445	2,145 ± 293
	VI	1,616 ± 176	1,991 ± 65	1,901 ± 174	1,503 ± 138
Ecl	II	2,337 ± 204	2,602 ± 381	2,453 ± 214	2,672 ± 206
	III	2,754 ± 497	2,762 ± 235	2,386 ± 283	2,150 ± 139
	V	1,659 ± 206	2,522 ± 324	2,111 ± 269	2,188 ± 125
	VI	1,523 ± 236	1,788 ± 215	1,737 ± 132	1,424 ± 139

in Er, Elr, Ei, and Ecl, whereas it did not differ between newborn and 5–9-year-old monkeys in Elc and Ec.

Layer VI. The soma size of Layer VI neurons exhibited different postnatal developmental profiles in different subdivisions: age groups ($F_{(3,12)}$ = 21.881, p < .001, η^2_p = .845), subdivisions ($F_{(3.106,37.278)}$ = 5.779, p = .002, η^2_p = .325), interaction ($F_{(9.319,37.278)}$ = 3.644, p = .002, η^2_p = .477). The developmental profile of neuronal soma size exhibited a clear rostro-caudal gradient in Layer VI. There was an increase between birth and 6 months of age in Er, Elr, Ei, Elc, Ec, and Ecl, which was followed by a gradual decrease into adulthood. The soma size of Layer VI neurons was larger in 5–9-year-old than in newborn monkeys in Er and Ei, whereas it did not differ between newborn and 5–9-year-old monkeys in Elr, Elc, Ec, and Ecl.

3.3.3 | Analyses per layer within subdivisions

Eo. Neuronal soma size exhibited different postnatal developmental profiles in the different layers of Eo (Figure 4a): age groups ($F_{(3,12)}$ = 14.005, p < .001, η^2_p = .778), layers ($F_{(2,24)}$ = 59.478, p < .001, η^2_p = .832), interaction ($F_{(6,24)}$ = 3.807, p = .008, η^2_p = .488). In Layer II, there was a transient increase at 6 months and 1 year of age, and no difference between newborn and 5–9-year-old monkeys (p = .941). In Layers III and V–VI, there was an early increase between birth and 6 months of age, and no significant changes thereafter.

Er. Neuronal soma size exhibited different postnatal developmental profiles in the different layers of Er (Figure 4b): age groups ($F_{(3,12)}$ = 17.163, p < .001, η^2_p = .811), layers ($F_{(1.719,20.628)}$ = 47.191, p < .001, η^2_p = .797), interaction ($F_{(5.157,20.628)}$ = 9.162, p < .001, η^2_p = .696). Nevertheless, neurons in all layers exhibited a transient increase in soma size at 6 months of age, with a gradual decrease into adulthood. In Layer II, there was a large increase from birth to 6 months of age, followed by a gradual decrease toward 5–9-years of age when soma size was similar to that at birth. There were no statistically significant differences between age groups for Layer III neurons, even though neuronal soma size was larger in 6-month-old than in newborn (p = .069) and 5–9-year-old (p = .035) monkeys. In Layers V and VI, there was a large increase in neuronal soma size between

TABLE 5 Results of the statistical analyses on neuronal soma size ($\mu m^3 \pm SD$) in the different layers of the seven subdivisions of the rhesus monkey entorhinal cortex at four postnatal ages

		Profile	$F_{(3,12)}$	p	η^2_p	Post hoc comparisons
Eo	II	Transient	5.863	.011	.594	Newborn < 6-month — 1-year > 5–9-year
	III	Early increase	7.135	.005	.641	Newborn < 6-month — 1-year — 5–9-year
	V–VI	Early increase	12.066	.001	.751	Newborn < 6-month — 1-year — 5–9-year
Er	II	Transient	9.577	.002	.705	Newborn < 6-month > 1-year > 5–9-year
	III	Transient	2.233	.137	.358	Newborn < 6-month; 6-month > 5–9-year
	V	Transient increase	19.738	.000	.831	Newborn < other ages; 6-month > 5–9-year
	VI	Transient increase	19.007	.000	.826	Newborn < other ages; 6-month > 1-year — 5–9-year
Elr	II	Transient	4.194	.030	.512	Newborn < 6-month — 1-year; 6-month > 5–9-year
	III	Transient	6.105	.009	.604	Newborn < 6-month; 6-month — 1-year > 5–9-year
	V	Transient increase	14.565	.000	.785	Newborn < other ages; 6-month — 1-year > 5–9-year
	VI	Transient	7.747	.004	.659	Newborn < 6-month — 1-year > 5–9-year
Ei	II	Two-step increase	16.170	.000	.802	Newborn < 6-month — 1-year < 5–9-year
	III	Transient	2.900	.079	.420	Newborn < 6-month; 6-month > 5–9-year
	V	Transient increase	23.170	.000	.853	Newborn < other ages; 6-month > 5–9-year
	VI	Transient increase	22.242	.000	.848	Newborn < other ages; 6-month — 1-year > 5–9-year
Elc	II	Transient	8.603	.003	.683	Newborn < 6-month — 1-year > 5–9-year
	III	Late decrease	6.251	.008	.610	Newborn — 6-month — 1-year > 5–9-year
	V	Transient	6.118	.009	.605	Newborn < 6-month — 1-year; 6-month > 5–9-year
	VI	Transient	11.561	.001	.743	Newborn < 6-month — 1-year > 5–9-year
Ec	II	No change	0.900	.469	.184	None significant
	III	Late decrease	10.065	.001	.716	Newborn — 6-month — 1-year > 5–9-year
	V	Transient	7.153	.005	.641	Newborn < 6-month — 1-year > 5–9-year
	VI	Transient	10.069	.001	.716	Newborn < 6-month — 1-year > 5–9-year
Ecl	II	No change	1.317	.315	.248	Newborn < 5–9-year
	III	Gradual decrease	3.560	.047	.471	Newborn — 6-month > 5–9-year
	V	Transient increase	8.597	.003	.682	Newborn < other ages; 6-month > 5–9-year
	VI	Transient	3.451	.051	.463	Newborn < 6-month; 6-month — 1-year > 5–9-year

birth and 6 months of age ($p < .001$), followed by a gradual decrease leading to a smaller neuronal soma size in 5–9-year-old than in 6-month-old monkeys (both $p < .05$); soma size of Layers V and VI neurons was larger in 5–9-year-old than in newborn monkeys (both $p < .001$).

Elr. Neuronal soma size exhibited different postnatal developmental profiles in the different layers of Elr (Figure 4c): age groups ($F_{(3,12)]} = 10.933$, $p = .001$, $\eta^2_p = .732$), layers ($F_{(3,36)} = 39.981$, $p < .001$, $\eta^2_p = .769$), interaction ($F_{(9,36)} = 3.106$, $p = .007$, $\eta^2_p = .437$). Nevertheless, neurons in all layers exhibited a transient increase at 6 months of age, with a gradual decrease into adulthood. Neuronal soma size did not differ between newborn and 5–9-year-old monkeys in Layers II, III, and VI, but it was larger in 5–9-year-old than in newborn monkeys in Layer V ($p = .030$).

Ei. Neuronal soma size exhibited different postnatal developmental profiles in the different layers of Ei (Figure 4d): age groups ($F_{(3,12)} = 16.829$, $p < .001$, $\eta^2_p = .808$), layers ($F_{(3,36)} = 34.986$, $p < .001$, $\eta^2_p = .745$), interaction ($F_{(9,36)} = 10.908$, $p < .001$, $\eta^2_p = .732$). Layer II neurons exhibited a gradual increase from birth to 5–9 years of age. Layer III neurons exhibited a transient increase at 6 months of age, although the overall age difference failed to reach statistical significance. Layers V and VI neurons exhibited a transient increase from birth until at least 6 months of age, followed by a gradual decrease into adulthood; soma size of Layers V and VI neurons were larger in 5–9-year-old than in newborn monkeys (both $p < .005$).

Elc. Neuronal soma size exhibited different postnatal developmental profiles in the different layers of Elc (Figure 4e): age groups ($F_{(3,12)} = 8.123$, $p = .003$, $\eta^2_p = .670$), layers ($F_{(3,36)} = 41.674$, $p < .001$, $\eta^2_p = .776$), interaction ($F_{(9,36)} = 5.044$, $p < .001$, $\eta^2_p = .558$). Nevertheless, neurons from all layers exhibited a transient increase from birth until at least 6 months of age, followed by a gradual decrease into adulthood. Neuronal soma size did not differ between newborn and 5–9-year-old monkeys in Layers II, V, and VI. In contrast, neuronal soma size was smaller in 5–9-year-old monkeys than in younger monkeys in Layer III.

Ec. Neuronal soma size exhibited different postnatal developmental profiles in the different layers of Ec (Figure 4f): age groups ($F_{(3,12)}$ = 7.737, p = .004, η^2_p = .659), layers ($F_{(1.658,19.896)}$ = 54.463, p < .001, η^2_p = .819), interaction ($F_{(4.974,19.896)}$ = 5.691, p < .001, η^2_p = .587). Layer II neurons did not exhibit age-related changes in soma size. Layer III neurons exhibited a decrease between 1 year and 5–9 years of age, whereas neurons in Layers V and VI exhibited a transient increase until at least 6 months of age, followed by a gradual decrease into adulthood. Neuronal soma size did not differ between newborn and 5–9-year-old monkeys in Layers V and VI.

Ecl. Neuronal soma size exhibited different postnatal developmental profiles in the different layers of Ecl (Figure 4g): age groups ($F_{(3,12)}$ = 2.516, p = .108, η^2_p = .386), layers ($F_{(3,36)}$ = 82.145, p < .001, η^2_p = .873), interaction ($F_{(9,36)}$ = 6.419, p < .001, η^2_p = .616). Layer II neurons did not exhibit age-related changes in soma size. Layer III neurons exhibited a gradual decrease from 6 months to 5–9 years of age, whereas neurons in Layers V and VI exhibited a transient increase until at least 6 months of age, followed by a gradual decrease into adulthood. Neuronal soma size was larger in 5–9-year-old than in newborn monkeys in Layer V, whereas it did not differ between newborn and 5–9-year-old monkeys in Layer VI.

4 | DISCUSSION

Consistent with findings on the structural development of the hippocampal formation (Jabès et al., 2010, 2011), the different layers and neurons of the seven subdivisions of the monkey entorhinal cortex exhibit different postnatal developmental profiles. Importantly, the developmental profiles observed in the different layers and subdivisions of the entorhinal cortex parallel the developmental profiles observed in the hippocampal structures with which they are interconnected. Since the fundamental features of the laminar and topographical organization of the entorhinal cortex projections to the hippocampal formation are similar to those of adults by 2 weeks of age in rhesus monkeys (Amaral et al., 2014), the current findings may shed light on the differential structural maturation of putative functional circuits supporting the interactions between the entorhinal cortex and the rest of the hippocampal formation.

4.1 | Neuron number

As expected, we did not find age-related differences in neuron numbers in the postnatal monkey entorhinal cortex. Our estimates in monkeys from birth to 1 year of age were consistent with our previous results in adult monkeys (Piguet et al., 2018). Indeed, neurons destined for the entorhinal cortex are generated by mid gestation in monkeys, following an inside-out spatio-temporal gradient (Nowakowski & Rakic, 1981; Rakic & Nowakowski, 1981). Deeply located neurons are generated before superficially located neurons. The production of neurons located in the deep layers of the entorhinal cortex ends around E56, whereas neurons destined for the superficial layers are generated up until E70. Since, to our knowledge, there is no developmental study on the number of neurons in the entorhinal cortex in either rats, monkeys or humans, we refer the reader to our previous publication for a comparison of our current results with previous studies in adult individuals (Piguet et al., 2018).

4.2 | Neuronal soma size

The average neuronal soma size exhibited different profiles of postnatal changes in distinct layers of different subdivisions of the rhesus monkey entorhinal cortex. Nevertheless, neuronal soma size typically increased between birth and 6 months of age, except in the superficial Layers II and III of Ec and Ecl. Neuronal soma size then typically decreased from 6 months to 5–9 years of age, except in Layer II of Ei where it increased until 5–9 years of age, as well as in Layer II of Ec and Ecl where it remained stable from birth until 5–9 years of age. These findings are interesting in light of the overproduction of synapses observed in several cortical regions between birth and approximately 4 months of age in rhesus monkeys (Rakic, Bourgeois, Eckenhoff, Zecevic, & Goldman-Rakic, 1986), and between birth and 15 months of age in humans (Huttenlocher & Dabholkar, 1997). Synapse overproduction is followed by a systematic elimination of synapses until adulthood, when synaptic density is often close to that observed at birth in both monkeys and humans, although the proportion of different types of synapses found in neonate and adult individuals may vary (Huttenlocher & Dabholkar, 1997; Rakic et al., 1986). In monkeys, synapse overproduction was reported to be nearly simultaneous in the motor, somatosensory, prefrontal, and visual cortices, as well as a limbic area, which may have included the entorhinal cortex. However, a detailed evaluation of Figure 2 in Rakic et al. (1986) suggests that the exact ages at which synapse overproduction reaches its peak may vary slightly in different cortical areas in monkeys, as in humans. In the sample derived from the limbic area, the peak density of synapses per 100 μm^2 of neuropil occurred around 5 to 6 months of age. It stands to reason that increased synaptic density is accompanied by a corresponding increase in neuronal soma size (Beul & Hilgetag, 2019). This is essentially what we observed in most layers of most subdivisions of the entorhinal cortex between birth and 6 months of age. However, our data on neuronal soma size also suggest that following an initial increase the structural maturation of neurons follows different time courses in distinct layers of different subdivisions of the entorhinal cortex. Our findings in the monkey entorhinal cortex are thus consistent with a study in humans (Rabinowicz, Petetot, Khoury, & de Courten-Myers, 2009), which reported that changes in neuronal soma size from adolescence to young adulthood was also specific to, and may differ between, distinct layers in different cortical areas.

4.3 | Differential development of distinct subdivisions

We found various age-related differences in neuronal soma size in, and volume of, distinct layers in different subdivisions of the monkey

entorhinal cortex. As shown in the hippocampus, postnatal changes in the volume of individual layers or structures are correlated with functional changes revealed by genome-wide patterns of gene expression (Favre et al., 2012a, 2012b; Jabès et al., 2010, 2011; Lavenex et al., 2004, 2007; Lavenex et al., 2014). In the entorhinal cortex, we found postnatal changes in neuronal soma size that often included a transient increase at 6 months of age. Although soma size is not sufficient by itself to reflect the functional maturation of neurons, changes in neuronal soma size together with volumetric changes of individual layers may provide information on the structural development of putative functional circuits to which these neurons contribute. We now review our main findings for each subdivision of the entorhinal cortex, and consider the changes in volume of each layer with the changes in neuronal soma size (Figure 5).

4.3.1 | Eo

Eo is the only subdivision of the entorhinal cortex that receives a direct unimodal input from the olfactory bulb (Insausti et al., 1987). In addition, Eo has limited interconnections with other subdivisions of the entorhinal cortex and projects to the rostral portion of the hippocampus and dentate gyrus (Witter & Amaral, 1991). Kesner (2013) reported that in rats, the ventral dentate gyrus, which corresponds to the rostral dentate gyrus in primates, contributes to odor pattern separation. We have shown in monkeys that there are 4–5 times more neurons in the superficial layers than in the deep layers of Eo, and that there are about 5–7 times more neurons in Layer III than in Layer II. Accordingly, since the targets of the projection of Layer II neurons, the dentate gyrus granule cells, exhibit a rather late maturation extending beyond 1 year of age in monkeys (Jabès et al., 2010, 2011), the direct projection from Layer III neurons to CA1 may contribute to the encoding of odors as contextual information in early hippocampus-dependent memories. With the late maturation of the granule cells pattern separation for odor information might become more specific and help disambiguate closely related odors enabling the encoding of more distinct memories. Within the hippocampus, we also observed a two-step maturational process, with CA1 maturing before CA3 (Favre et al., 2012a; Jabès et al., 2010, 2011; Lavenex, Sugden, Davis, Gregg, & Lavenex, 2011). Accordingly, whereas neuronal somas reached adult-like size by 6 months of age in Layers III and V–VI, the volumes of Layers III and V–VI increased between birth and 6 months of age and again after 1 year of age. In contrast, whereas the volume of Layer II did not change with age, the soma size of Layer II neurons decreased after 1 year of age to become adult-like. Altogether, these results suggest that the two-step maturation of intra-hippocampal circuits may contribute to the two-step maturation of Eo, via feedback projections from CA1 and the subiculum, and via intrinsic deep-to-superficial projections within the entorhinal cortex (Chrobak & Amaral, 2007). Eo also receives some more minor projections from the basal, accessory basal, and paralaminar nuclei of the amygdala, which are restricted to Layers III and V–VI. The protracted maturation of the amygdala, which we reported previously (Chareyron et al., 2012), may thus also contribute to the structural changes observed in Eo.

4.3.2 | Er

Er receives the majority of its cortical afferents from Layer III neurons of the perirhinal cortex, which terminate most strongly in Layers I, II, and the superficial portion of Layer III. Although Er sends relatively

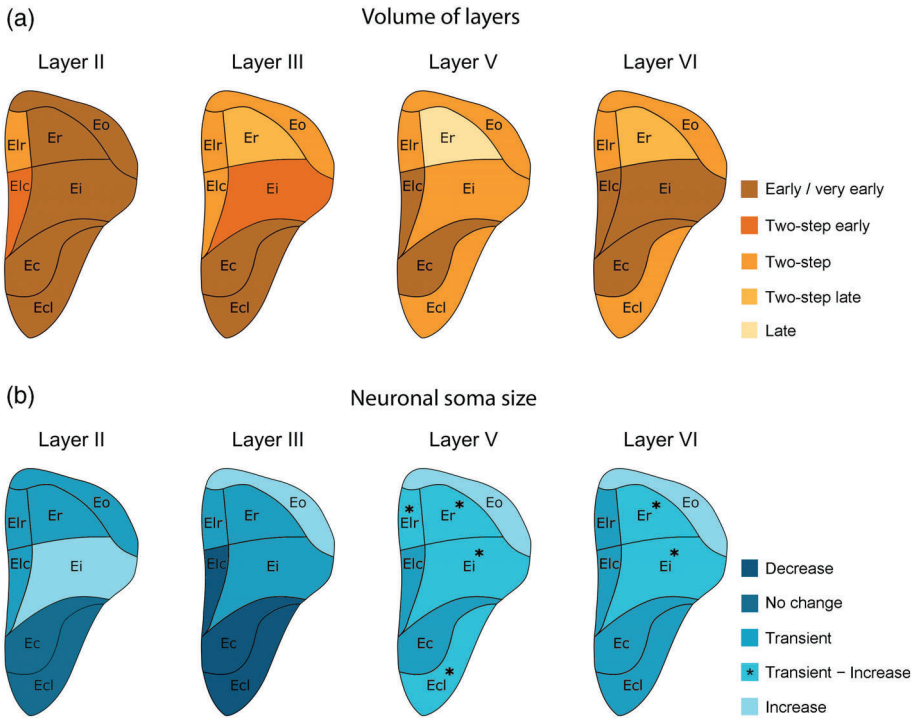

FIGURE 5 Summary of the different profiles of postnatal development in the seven subdivisions of the monkey entorhinal cortex. (a) Volume of distinct layers. (b) Neuronal soma size in distinct layers. See main text for details [Color figure can be viewed at wileyonlinelibrary.com]

fewer feedback projections to the perirhinal cortex (as compared to Elr and more caudal subdivisions) (Suzuki & Amaral, 1994), these projections originate mainly from cells located in Layer V, which is also the recipient of hippocampal projections. Er receives the heaviest input from the lateral and basal nuclei of the amygdala, with fibers and terminals located in all layers, but most heavily in Layers III, V, and VI (Pitkänen et al., 2002). Er also receives projections from the parvicellular division of the accessory basal nucleus. In monkeys, the lateral, basal, and accessory basal nuclei exhibit a large increase in volume between birth and 3 months of age, followed by a slower growth continuing beyond 1 year of age (Chareyron et al., 2012). In contrast, the paralaminar nucleus contains a large pool of immature neurons that gradually develop into mature neurons, leading to a late increase in volume of this nucleus. Although it is difficult to draw strict parallels between the postnatal development of the hippocampal formation (Jabès et al., 2010, 2011) and that of the amygdala (Chareyron et al., 2012), the interconnections with both structures likely influence the structural maturation of Er. Altogether, our data indicate that the layers of Er that receive major cortical inputs from the perirhinal cortex mature first, and that the maturation of Layer III may also be influenced by the maturation of the amygdala projections and the feedback projections from the hippocampus reaching Layer V. In contrast to what was observed in the caudal portion of the entorhinal cortex, the deep layers of Er are rather late developing and may therefore be particularly dependent on the conjunctive maturation of amygdala and hippocampal projections.

4.3.3 | Elr

The development of Elr is very similar to that of Er, not surprisingly since both areas exhibit similar connectivity with the perirhinal cortex, the hippocampal formation and the amygdala, with the exception of fewer projections from the paralaminar nucleus in Elr (Pitkänen et al., 2002). In addition, Elr is more highly interconnected with the caudal hippocampus, whereas Er is more highly interconnected with the mid portion of the hippocampus (Chrobak & Amaral, 2007; Witter & Amaral, 1991). Nevertheless, such differences do not appear to be reflected in major differences in the structural development of the distinct layers and neurons in these two subdivisions. Altogether, our data indicate that the layers of Elr that receive major cortical inputs from the perirhinal cortex mature first, and that the maturation of Layer III may also be influenced by both the maturation of the amygdala projections and the feedback projections from the hippocampus reaching Layer V. In contrast to what was observed in the caudal entorhinal cortex, the deep layers of Elr are developing later, perhaps in relation to the conjunctive maturation of amygdala and hippocampal projections.

4.3.4 | Ei

Ei shares some structural and functional characteristics with both the rostral and caudal subdivisions of the entorhinal cortex. Ei receives prominent projections from Layer III neurons of the perirhinal and parahippocampal cortices, which terminate most heavily in Layers I–III. In contrast to Ec and Ecl, Ei does not receive any projections from the presubiculum. In addition, the rostral half of Ei receives projections from the lateral nucleus of the amygdala, with the densest labeling in Layer III (Pitkänen et al., 2002). Very light projections from the parvicellular divisions of the basal and accessory basal nuclei also reach the rostral half of Ei. It is therefore not surprising that Ei exhibited a developmental profile that was intermediate between those observed in more rostral subdivisions, in particular Er, and those observed in more caudal subdivisions, in particular Ec. Layers I and II exhibited an early maturation, consistent with an early maturation of the cortical inputs reaching the entorhinal cortex. In contrast to Eo, Er, and Elr, but in accordance with Elc and Ec, Ei exhibited an early volumetric maturation of Layer I and VI and a transient increase of neuronal soma size in Layer VI. Interestingly, these layers and regions are reciprocally connected with the retrosplenial cortex (Insausti et al., 1987; Insausti & Amaral, 2008; Kobayashi & Amaral, 2003, 2007). In turn, the retrosplenial cortex is interconnected with the presubiculum and the parasubiculum (Kobayashi & Amaral, 2003, 2007), which both exhibit a very early maturational profile (Jabès et al., 2010, 2011; Lavenex et al., 2004, 2007). Accordingly, the complex patterns of postnatal development of Ei likely reflect the complexity of its interconnections with various brain regions involved in distinct functional networks.

4.3.5 | Elc

Elc receives projections from Layer III neurons of the perirhinal cortex, the rostral parahippocampal cortex, anterior cingulate cortex, and the superior temporal gyrus, which terminate most strongly in Layers I and III (Insausti & Amaral, 2008). Elc also receives prominent projections from the prefrontal cortex, which terminate in Layer VI. Overall, Elc exhibited an early volumetric maturation profile. And, despite subtle differences between layers, all of its layers appeared to exhibit an early maturation profile. Neurons in all layers of Elc exhibited a transient increase in soma size from birth until at least 6 months of age, followed by a gradual decrease into adulthood. The developmental profile of Elc was thus somewhat intermediate between those of Elr and Ec, and distinct from the adjacent medially situated Ei.

4.3.6 | Ec

Ec receives prominent projections from Layer III neurons of the parahippocampal cortex, which terminate most strongly in Layers I–III (Suzuki & Amaral, 1994). In addition, Ec is characterized by a direct projection from the presubiculum to Layer III. The connections between the entorhinal cortex and the parahippocampal cortex are highly reciprocal. Feedback projections originate mainly from Layer V neurons in Ec, with fewer Layer VI neurons and occasional Layer III neurons. Layers V and VI of Ec exhibited an early maturation.

Accordingly, our current findings suggest that some putative functional circuits within Ec and with some interconnected brain regions including the presubiculum and the parahippocampal cortex may mature early. Since both the presubiculum and the parahippocampal cortex are interconnected with the retrosplenial cortex (Kobayashi & Amaral, 2003, 2007), it would be interesting to determine whether these two cortical areas exhibit developmental profiles corresponding to those observed in Ec and the presubiculum (Jabès et al., 2011).

4.3.7 | Ecl

Similar to Ec, Ecl receives prominent projections from Layer III neurons of the parahippocampal cortex, which terminate most strongly in Layers I–III, as well as a direct projection from the presubiculum to Layer III (Suzuki & Amaral, 1994). Accordingly, the maturation profile of Layers I–III was similar in Ec and Ecl. In contrast, Layers V and VI of Ecl exhibited a delayed maturation profile as compared to Layers V and VI of Ec. Thus, although Ec and Ecl share some common connectional characteristics and functional properties, they differ not only in the relative numbers of superficial neurons contributing to different hippocampal circuits (Piguet et al., 2018), but also in the maturation profile of their deep Layers V and VI, which receive feedback projections from CA1 and the subiculum, as well as projections from several cortical areas (Insausti et al., 1987; Insausti & Amaral, 2008).

4.4 | Differential development of individual layers

Although the postnatal development of distinct layers differed between subdivisions, overall the superficial layers developed earlier than the deep layers. This was particularly the case in the rostral portion of the entorhinal cortex, suggesting that the postnatal maturation of the deep layers may be more highly dependent on the feedback projections from CA1 and the subiculum in the rostral entorhinal cortex. In contrast, the maturation of the deep layers of the caudal portion of the entorhinal cortex may be associated to the maturation of functional circuits including projections from the presubiculum and its interconnections with the retrosplenial cortex, also via the parahippocampal cortex. Here, we compare the postnatal development of individual layers between subdivisions.

4.4.1 | Layer I

Layer I receives cortical afferents and contains the dendrites of entorhinal cortex neurons. Despite subtle differences between subdivisions, the volumetric development of Layer I exhibited an early or very early maturation profile. The vast majority of cortical afferent projections to the entorhinal cortex terminate in Layers I–III (Insausti & Amaral, 2008). In addition, the intrinsic connections of the entorhinal cortex terminate predominantly in Layers III and I (Chrobak & Amaral, 2007), which contain the dendrites of many neurons from Layers II, III, and V (Buckmaster, Alonso, Canfield, & Amaral, 2004). Consequently, it is difficult to draw clear inferences regarding the maturation of specific circuits based on the postnatal developmental profile of Layer I. However, since Layer I is one of the main termination layers of cortical afferents, sensory inputs reaching Layer I may contribute to its volumetric maturation by 6 months of age in all subdivisions.

4.4.2 | Layer II

Layer II receives cortical afferents and the majority of its principal neurons project to the dentate gyrus, CA3, and CA2 (Ohara et al., 2019; Witter et al., 2017). Despite some peculiar differences in Elr and Elc, the postnatal volumetric development of Layer II exhibited an early maturation profile. In contrast, the postnatal developmental profile of neuronal soma size exhibited a clear rostro-caudal gradient, with a transient increase at 6 months and 1 year of age in Eo, Er, Elr, and Elc, a two-step increase from birth to adulthood in Ei, and no significant changes in Ec and Ecl. Since Layer II is one of the main termination layers of cortical afferents, it is tempting to consider that sensory inputs reaching Layer II contribute to the volumetric maturation of this layer, and that this maturation is relatively complete by 6 months of age in all subdivisions. Although different cortical afferents terminate in different subdivisions of the entorhinal cortex, they do not seem to have a differential impact on the postnatal volumetric development of Layer II. However, in addition to the neocortical projections reaching Layer II, Layer II is also the recipient of direct projection from the parasubiculum, which exhibits a very early maturation profile (Jabès et al., 2011). We may thus conclude that both sets of inputs may contribute to this early maturation.

In contrast, postnatal changes in neuronal soma size suggest that the maturation of the principal circuits involving Layer II neurons, namely the projections to the dentate gyrus, CA3, and CA2, varies between subdivisions. Indeed, Layer II comprises several cell types including, but not limited to, stellate and pyramidal cells (Amaral & Lavenex, 2007; Buckmaster et al., 2004). Quantitative data on the proportion of these different cell types in the rodent medial entorhinal cortex revealed that the majority of these neurons are stellate cells (rat: 81% (Schwartz & Coleman, 1981); rat: 67%, mouse: 74% (Gatome, Slomianka, Lipp, & Amrein, 2010)). In rats, principal cells in Layer II come in two chemical types: reelin and calbindin expressing cells (Ohara et al., 2019). Reelin-positive stellate cells are the exclusive origin of the entorhinal cortex projections to the dentate gyrus, CA2, and CA3. Calbindin-positive pyramidal neurons provide excitatory input to the reelin-positive stellate cells both directly and indirectly (Witter et al., 2017). We did not consider the cytoarchitectonic criteria defined in Nissl-stained sections for rodents to be sufficiently reliable to define distinct neuronal phenotypes that would be consistent across different subdivisions of the monkey entorhinal cortex. Nevertheless, the maturation of both Layer II stellate and pyramidal cells together likely contributes to the increased influence of the trisynaptic pathway, as compared to the direct projection from Layer III neurons to CA1, during early postnatal development.

The transient increase in neuronal soma size in Eo, Er, Elr, and Elc is consistent with the initial overproduction of synapses around 6 months of age, followed by their selective elimination (Rakic et al., 1986). In contrast, neuronal soma size remained stable between birth and adulthood in Ec and Ecl, suggesting that the initial synapse overproduction and subsequent elimination may occur prior to birth in these areas. Finally, neuronal soma size exhibited a two-step increase between birth and adulthood in Ei, revealing that its Layer II neurons did not follow the same developmental pattern observed in other subdivisions. The patterns of amygdala projections within different subdivisions of the entorhinal may explain these differences. Indeed, amygdala projections terminate predominantly in Layer II in Ei, whereas amygdala projections terminate in Layers III and V in Eo and Er, and there are no amygdala projections to Ec and Ecl.

The dentate gyrus, one of the main targets of entorhinal cortex Layer II neuron projections, exhibits a protracted period of neuron addition that is accompanied by a late maturation of its granule cell population, which continues beyond the first postnatal year in monkeys (Jabès et al., 2010, 2011). Our results in the rostral entorhinal cortex are consistent with the results in the dentate gyrus. In contrast, our results in the caudal entorhinal cortex suggest an early maturation of Layer II neurons. Interestingly, the projections from the caudal entorhinal cortex terminate predominantly in the middle third of the molecular layer of the dentate gyrus and in the outer portion of stratum lacunosum-moleculare of CA3 and CA2, whereas the projections from the rostral entorhinal cortex terminate predominantly in the outer third of the molecular layer and the inner portion of stratum lacunosum-moleculare of CA3 and CA2 (Amaral et al., 2014; Witter & Amaral, 1991). Accordingly, the projections from Ec and Ecl may have an earlier and stronger influence on information processing in the developing dentate gyrus, CA3, and CA2 than the projections from the other subdivisions of the entorhinal cortex, which mature later and terminate more distally on the dendrites of the dentate granule cells and the pyramidal neurons of CA3 and CA2.

4.4.3 | Layer III

Layer III neurons receive cortical afferents and project to CA1 and the subiculum. The postnatal volumetric development of Layer III exhibited a clear rostro-caudal gradient, with a two-step/late maturation profile in Er, a two-step maturation profile in Eo and Elr, a gradual maturation profile in Elc, a two-step/early maturation profile in Ei, and an early maturation profile in Ec and Ecl. Similarly, the postnatal developmental profile of neuronal soma size exhibited a clear rostro-caudal gradient in Layer III, with an increase between birth and 6 months of age in Eo, after which soma size remained stable; an increase between birth and 6 months of age, followed by a gradual decrease of soma size into adulthood in Er, Elr, and Ei; and a decrease in soma size after 6 months of age in Elc, Ec, and Ecl.

Similar to Layers I and II, Layer III is the recipient of various cortical projections, which are preferentially directed toward different subdivisions. Projections from the perirhinal cortex terminate predominantly in Eo, Er, Elr, Elc, and the rostral part of Ei. Projections from the parahippocampal cortex, in contrast, terminate predominantly in Ec and Ecl, and the caudal part of Ei. Projections from the insula, the orbitofrontal cortex, and the anterior cingulate cortex are directed predominantly toward Eo, Er, Elr, and Ei, whereas projections from the retrosplenial cortex and the superior temporal gyrus are directed predominantly toward Ei, Ec, and Ecl. Projections from the amygdala are directed toward Eo, Er, Elr, and the rostral portions of Ei and Elc, with essentially no amygdala projections to Ec and Ecl (Pitkänen et al., 2002). In contrast to what was observed in Layer II, the postnatal development of Layer III suggests that the structural development of different subdivisions of the entorhinal cortex, which may be involved in the processing of different types of information, exhibit different maturation profiles. The caudal entorhinal cortex matures relatively early, whereas the rostral entorhinal cortex matures relatively late.

The main targets of entorhinal cortex Layer III neurons projections, CA1 and the subiculum, exhibit a relatively early maturation already by 6 months of age (Jabès et al., 2011; Lavenex et al., 2004; Lavenex et al., 2011). In particular, stratum lacunosum-moleculare of CA1, which is the target of the direct entorhinal cortex projection, exhibits an earlier maturation than the other layers of CA1. Similarly, the molecular layer of the subiculum, which receives direct projections from the entorhinal cortex matures earlier than the rest of the subiculum. Interestingly, the direct connections between the entorhinal cortex and CA1 and the subiculum are largely reciprocal. The relative segregation of these reciprocal connections suggests that the maturation of separate hippocampal circuits may be related to the type of information being processed and thus may exhibit differential patterns along the transverse axis of the hippocampus during postnatal development. In addition, in Ec and Ecl, we found that neuronal soma size was larger at birth, 6 months, and 1 year of age, as compared to 5–9 years of age. Interestingly, Layer III of Ec and Ecl is the recipient of direct projections from the presubiculum, which exhibits a similar developmental pattern (Jabès et al., 2011).

4.4.4 | Layer V

Layer V neurons receive feedback projections from the hippocampus and subiculum. The postnatal volumetric development of Layer V exhibited differences between subdivisions, but these differences did not appear to follow a clear rostro-caudal gradient. Eo, Ei, and Elr exhibited a two-step maturation profile, Er exhibited a late maturation profile, Elc and Ec exhibited an early maturation profile, and Ecl exhibited an early-late maturation profile. In contrast, the postnatal developmental profile of neuronal soma size exhibited a clear rostro-caudal gradient in Layer V. There was an increase in soma size of Layers V–VI neurons between birth and 6 months of age in Eo, after which soma size remained stable; and an increase in neuronal soma size between birth and 6 months of age, followed by a gradual decrease thereafter in all other subdivisions. Neuronal soma size was smaller in newborn than in 5–9-year-old monkeys in Er, Elr, Ei, and Ecl, whereas it did not differ between newborn and 5–9-year-old monkeys in Elc and Ec.

Layer V is the main recipient of hippocampal output via feedback projections from CA1 and the subiculum, which are topologically in register with the projections of Layer III neurons to the hippocampus and subiculum. However, Layer V neurons are also the recipients of different cortical afferents in different subdivisions of the entorhinal cortex, which may further influence their structural development. Specifically, Layer V neurons in Er and Elr receive some projections from the orbitofrontal cortex, whereas Layer V neurons in Ei, Ec, and Ecl receive some projections from the parahippocampal and retrosplenial cortices. Furthermore, as was shown in the rodent medial entorhinal cortex (which corresponds to the caudal entorhinal cortex areas Ec and Ecl in primates), Layer V neurons may receive direct inputs from the presubiculum and parasubiculum onto their apical dendrites in Layers III and II (respectively; Canto, Koganezawa, Beed, Moser, & Witter, 2012), as well as a direct input from entorhinal cortex Layer II stellate cells that contribute the main projection to the dentate gyrus, CA3, and CA2 (Surmeli et al., 2015). Accordingly, different sets of cortical projections may have a differential impact on the structural maturation of Layer V neurons in different subdivisions of the entorhinal cortex. It would be interesting to obtain similar information on the structural development of the cortical areas projecting to Layer V, principally the orbitofrontal, parahippocampal, and retrosplenial cortices, to determine whether these areas exhibit similar developmental profiles.

4.4.5 | Layer VI

It is also interesting to consider the postnatal structural development of Layer VI in light of the different sets of cortical inputs reaching different subdivisions of the entorhinal cortex (Insausti & Amaral, 2008). In Er and Elr, Layer VI is the recipient of direct projections from the insula, as well as the orbitofrontal and medial prefrontal cortices. In Ei and Ec, Layer VI is the recipient of direct projections from the retrosplenial cortex, as well as the orbitofrontal and medial prefrontal cortices. In Elc, Layer VI is the recipient of direct projections from the orbitofrontal and medial prefrontal cortices. In Ecl, Layer VI is the recipient of direct projections from the orbitofrontal and retrosplenial cortices. In rats, Layer VI neurons of the medial entorhinal cortex also receive direct projections from the presubiculum and the parasubiculum (Canto et al., 2012). Based on these patterns of connectivity, the early maturation of Layer VI in Ec and Ecl may be linked to functional circuits involving the presubiculum, parasubiculum, and the retrosplenial cortex. In contrast, the additional influence of the structural development of functional circuits involving cortical regions in the frontal lobe may be more difficult to link to the specific patterns observed in Layer VI of the entorhinal cortex.

4.5 | Functional implications

We previously proposed that the differential maturation of distinct hippocampal circuits contributes to the emergence of different hippocampus-dependent memory processes (Lavenex & Banta Lavenex, 2013). Here, we have shown that different layers and subdivisions of the monkey entorhinal cortex exhibit different profiles of structural development, thus further suggesting that different networks processing different types of information mature at different times during early postnatal life. Most interestingly, the developmental profiles observed in the different layers and subdivisions of the entorhinal cortex parallel the developmental profiles observed in the hippocampal structures with which they are directly interconnected (Jabès et al., 2010, 2011). Now, we discuss the types of learning and memory processes that may be subserved by these networks, mainly based on electrophysiological and behavioral studies in rodents, and consider the potential implications of our findings for the emergence and development of spatial and episodic memory in humans.

4.5.1 | Path integration

Consistent with our earlier model linking the early development of the subiculum, presubiculum, and parasubiculum with the early emergence of path integration (Lavenex & Banta Lavenex, 2013), we found that Ec and Ecl exhibited an early structural development. As described above, Ec and Ecl are interconnected with a functional network including the subiculum, presubiculum, parasubiculum, retrosplenial, and parahippocampal cortices. These brain regions contain several cell types that contribute to spatial information processing, including place cells, head direction cells, grid cells, and boundary cells (Taube, 2007). During development, head-direction cells in the presubiculum and parasubiculum are the first to exhibit adult-like activity patterns (Langston et al., 2010). Hippocampal place cells evolve more gradually, whereas entorhinal cortex grid cells exhibit the slowest development. Interestingly, most cells in Layer III of the medial entorhinal cortex exhibit directional preferences at a very young age, as is the case in adult individuals (Langston et al., 2010). Altogether, these cells may support path integration, which can be defined as a computational process by which an organism continually monitors its own movement (Taube, 2007), or an internal computation that transforms a sense of motion into a sense of location (Savelli & Knierim, 2019). The inputs necessary for such a computation are essentially derived from self-motion cues produced by locomotion (Cullen & Taube, 2017). However, path integration is an imprecise mechanism, and errors will accumulate over time in absence of an external reference. Accordingly, the head direction signal must be periodically updated or recalibrated with respect to environmental landmarks. Importantly, visual calibration does not depend on visual information derived from the postrhinal cortex (Peck & Taube, 2017), which corresponds to the parahippocampal cortex in primates and is thought to be implicated in processing visual scene information (Epstein, 2008). Instead, the visual information necessary to maintain the calibration of the head direction system is derived from direct projections from the visual cortex to the presubiculum, which then exerts top-down control at the level of the lateral mammillary nuclei (Yoder, Peck, & Taube, 2015). Accordingly, path integration may enable

rodents and primates to successfully update their position and navigate in their environment before either visual scene information dependent on the parahippocampal cortex, or a basic allocentric spatial representations dependent on the functional maturation of CA1, become available. We therefore propose that the functional maturation of this discrete network including the subiculum, presubiculum, parasubiculum, and the caudal entorhinal cortex may underlie the emergence of path integration abilities in children between 6 and 12 months of age (Acredolo, 1978; Bremner, Knowles, & Andreasen, 1994; Rieser & Heiman, 1982).

4.5.2 | Basic allocentric spatial processing

Consistent with our earlier model linking the maturation of CA1 with the emergence of basic allocentric spatial processing and the offset of infantile amnesia (Lavenex & Banta Lavenex, 2013), Ec and Ecl exhibited an early structural development, between birth and 6 months of age, which is similar to what we observed in CA1 at the structural and molecular levels (Favre et al., 2012a; Jabès et al., 2011; Lavenex et al., 2011). Similarly, Ei exhibited a first volumetric increase between birth and 6 months of age, followed by a second increase after 1 year of age. In contrast, Er exhibited a late volumetric increase after 1 year of age, which was largely due to the development of its Layers III, V, and VI. Research in rodents demonstrated that CA1 place cell activity and a basic allocentric representation of the environment can be subserved by the direct monosynaptic pathway from the entorhinal cortex to CA1 (Brun et al., 2002). We therefore propose that the maturation of the reciprocal connections between the caudal entorhinal cortex and CA1 may underlie the emergence of allocentric spatial processing, which is reliably observed in children at 2 years of age (Newcombe, Huttenlocher, Bullock Drummey, & Wiley, 1998; Ribordy et al., 2013; Ribordy Lambert et al., 2015).

The bi-directional interaction between the hippocampus and the caudal entorhinal cortex may be critical to support this capacity. Grid cells found in the rat medial entorhinal cortex require an excitatory input from the hippocampus in order to maintain their normal firing pattern (Bonnevie et al., 2013). In the absence of hippocampal signal, grid cells become head direction cells likely driven by direct inputs from the presubiculum. Similarly, we have shown in monkeys that normal activation of the caudal entorhinal cortex (Ec and Ecl) during spatial exploration is dependent on the integrity of the hippocampus (Chareyron, Banta Lavenex, Amaral, & Lavenex, 2017). These two studies, using different methodologies in different species, suggest that the caudal entorhinal cortex (i.e., medial entorhinal cortex in rodents) may not be fully functional in the absence of functional hippocampal circuits. Accordingly, we propose that the functional maturation of CA1 may contribute to the functional maturation of the caudal entorhinal cortex in support of basic allocentric spatial processing (i.e., beyond its ability to support path integration via its interconnections with the subiculum, presubiculum, and parasubiculum). Such functional maturation includes the ability to integrate visual scene information provided by the parahippocampal cortex, which may enable the construction of low-resolution, allocentric spatial representations of the environment.

4.5.3 | Increased spatial memory precision and content

Consistent with our earlier model linking the protracted development of the dentate gyrus and CA3 with the age-related improvements in pattern separation which subserve high-resolution allocentric spatial representations (Lavenex & Banta Lavenex, 2013), we found that Er exhibited a late structural development after 1 year of age. The rostral entorhinal cortex (Er and the rostral part of Ei) receives significant projections from the amygdala and the perirhinal cortex (Pitkänen et al., 2002; Suzuki & Amaral, 1994). Accordingly, these two areas may be involved in the integration of emotional information, as well as the processing of local features related to individual items and objects, respectively. As proposed by Knierim et al. (2014), the lateral entorhinal cortex in rats, which corresponds to the rostral entorhinal cortex in primates, may be particularly involved in the processing of individual items and locations based on a local frame of reference, and provide the hippocampus with information about the content of an experience (Nilssen, Doan, Nigro, Ohara, & Witter, 2019). Similarly, Suzuki, Miller, and Desimone (1997) reported the activity of egocentric space-sensitive neurons in both the rostral and caudal entorhinal cortex recorded while monkeys were performing a delayed-matching-to-place task presented on a computer screen placed in front of them. Accordingly, rats with lesions of the lateral entorhinal cortex are impaired in their ability to learn a local spatial framework defined by an arrangement of small objects placed on the testing apparatus (Kuruvilla & Ainge, 2017).

In sum, the rostral entorhinal cortex may further contribute to the integration of spatial information about individual objects into a global representation of the environment. The rostral entorhinal cortex may thus contribute to increasing the precision of the spatial representation of the environment by integrating information about object locations, as well as provide the hippocampus with information about the content of an experience (Knierim et al., 2014). The late maturation of the rostral entorhinal cortex suggests that the increase in the content and precision of spatial and episodic memories develops progressively after the emergence of the ability to form a basic allocentric spatial representation, which is dependent on the maturation of the caudal entorhinal cortex (Lavenex & Banta Lavenex, 2013; Ribordy et al., 2013; Ribordy Lambert et al., 2015, 2016).

4.5.4 | Episodic memory

We previously proposed that the immaturity of the dentate gyrus may underlie the phenomenon of childhood amnesia, and that the gradual maturation of the trisynaptic hippocampal pathway subserves the gradual improvement, from 2 to 7 years of age, in our ability to create

autobiographical memories that can be recalled later in life (Lavenex & Banta Lavenex, 2013; Ribordy Lambert et al., 2015, 2016). Several mechanisms have been proposed to explain how hippocampal networks may represent moments in temporally organized experiences (Eichenbaum, 2017), but there was no clear indication regarding a specific contribution of the entorhinal cortex to the representation of time in support of episodic memory. However, a recent study by Tsao et al. (2018) reported that neurons in the rat lateral entorhinal cortex may provide a temporal signal that encodes time across multiple scales from seconds to hours, and may thus reflect the temporal structure of ongoing experience across different contexts. Accordingly, one may consider that the primate rostral entorhinal cortex may contribute to the definition of the temporal component of episodic memory. Together with the protracted maturation of the trisynaptic pathway, which is critical for rapid, single-trial contextual learning in support of the encoding of episodic memories, the late maturation of Er may contribute to the late improvement in our ability to create spatio-temporally distinct autobiographical memories.

4.6 | Conclusion

Consistent with our findings on the structural development of the hippocampal formation (Jabès et al., 2010, 2011), the different layers of the seven subdivisions of the monkey entorhinal cortex exhibit different postnatal developmental profiles. Most interestingly, the developmental profiles observed in the different layers and subdivisions of the entorhinal cortex parallel the developmental profiles observed in the hippocampal structures with which they are interconnected. Since the fundamental features of the laminar and topographical distributions of the entorhinal cortex projections to the hippocampal formation are largely similar to those of adults by 2 weeks of age in rhesus monkeys (Amaral et al., 2014), the current findings shed light on the differential structural maturation of putative functional circuits supporting the interactions between the entorhinal cortex and the rest of the hippocampal formation. The early maturation of the caudal entorhinal cortex may contribute to path integration and basic allocentric spatial processing, whereas the late maturation of the rostral entorhinal cortex may contribute to the increased precision of allocentric spatial representations and the temporal integration of individual items into episodic memories. Altogether, these results support the theory that the differential maturation of distinct hippocampal circuits contributes to the emergence of different hippocampus-dependent memory processes.

ACKNOWLEDGMENTS

This work was supported by Swiss National Science Foundation Grants P00A-106701, PP00P3-124536, and 310030_143956; US National Institutes of Health Grants MH041479 and NS16980; and California National Primate Research Center Grant OD011107.

DATA AVAILABILITY STATEMENT

The data that support the findings of this study are available from the corresponding author upon reasonable request.

ORCID

Olivia Piguet https://orcid.org/0000-0001-8398-0232
Loïc J Chareyron https://orcid.org/0000-0003-2043-3711
Pamela Banta Lavenex https://orcid.org/0000-0001-8868-2912
David G Amaral https://orcid.org/0000-0003-1525-8744
Pierre Lavenex https://orcid.org/0000-0002-9278-1312

REFERENCES

Acredolo, L. P. (1978). Development of spatial orientation in infancy. *Developmental Psychology*, *14*(3), 224–234.

Amaral, D. G., Insausti, R., & Cowan, W. M. (1987). The entorhinal cortex of the monkey: I. Cytoarchitectonic organization. *The Journal of Comparative Neurology*, *264*(3), 326–355.

Amaral, D. G., Kondo, H., & Lavenex, P. (2014). An analysis of entorhinal cortex projections to the dentate gyrus, hippocampus, and subiculum of the neonatal macaque monkey. *The Journal of Comparative Neurology*, *522*(7), 1485–1505. https://doi.org/10.1002/cne.23469

Amaral, D. G., & Lavenex, P. (2007). Hippocampal neuroanatomy. In P. Andersen, R. G. M. Morris, D. G. Amaral, T. V. Bliss, & J. O'Keefe (Eds.), *The hippocampus book* (pp. 37–114). Oxford: Oxford University Press.

Beul, S. F., & Hilgetag, C. C. (2019). Neuron density fundamentally relates to architecture and connectivity of the primate cerebral cortex. *NeuroImage*, *189*, 777–792. https://doi.org/10.1016/j.neuroimage.2019.01.010

Bonnevie, T., Dunn, B., Fyhn, M., Hafting, T., Derdikman, D., Kubie, J. L., … Moser, M. B. (2013). Grid cells require excitatory drive from the hippocampus. *Nature Neuroscience*, *16*(3), 309–317. https://doi.org/10.1038/nn.3311

Bremner, J. G., Knowles, L., & Andreasen, G. (1994). Processes underlying young children's spatial orientation during movement. *Journal of Experimental Child Psychology*, *57*(3), 355–376.

Brun, V. H., Otnass, M. K., Molden, S., Steffenach, H. A., Witter, M. P., Moser, M. B., & Moser, E. I. (2002). Place cells and place recognition maintained by direct entorhinal-hippocampal circuitry. *Science*, *296*(5576), 2243–2246.

Buckmaster, P. S., Alonso, A., Canfield, D. R., & Amaral, D. G. (2004). Dendritic morphology, local circuitry, and intrinsic electrophysiology of principal neurons in the entorhinal cortex of macaque monkeys. *The Journal of Comparative Neurology*, *470*(3), 317–329. https://doi.org/10.1002/cne.20014

Canto, C. B., Koganezawa, N., Beed, P., Moser, E. I., & Witter, M. P. (2012). All layers of medial entorhinal cortex receive presubicular and parasubicular inputs. *Journal of Neuroscience*, *32*(49), 17620–17631. https://doi.org/10.1523/Jneurosci.3526-12.2012

Carmer, S. G., & Swanson, M. R. (1973). Evaluation of 10 pairwise multiple comparison procedures by Monte-Carlo methods. *Journal of the American Statistical Association*, *68*(341), 66–74. https://doi.org/10.2307/2284140

Chareyron, L. J., Banta Lavenex, P., Amaral, D. G., & Lavenex, P. (2011). Stereological analysis of the rat and monkey amygdala. *The Journal of Comparative Neurology*, *519*(16), 3218–3239. https://doi.org/10.1002/cne.22677

Chareyron, L. J., Banta Lavenex, P., Amaral, D. G., & Lavenex, P. (2012). Postnatal development of the amygdala: A stereological study in macaque monkeys. *The Journal of Comparative Neurology*, *520*(9), 1965–1984. https://doi.org/10.1002/cne.23023

Chareyron, L. J., Banta Lavenex, P., Amaral, D. G., & Lavenex, P. (2017). Functional organization of the medial temporal lobe memory system following neonatal hippocampal lesion in rhesus monkeys. *Brain Structure & Function*, *222*(9), 3899–3914. https://doi.org/10.1007/s00429-017-1441-z

Chrobak, J. J., & Amaral, D. G. (2007). Entorhinal cortex of the monkey: VII. Intrinsic connections. *The Journal of Comparative Neurology*, *500*(4), 612–633. https://doi.org/10.1002/cne.21200

Cullen, K. E., & Taube, J. S. (2017). Our sense of direction: Progress, controversies and challenges. *Nature Neuroscience*, *20*(11), 1465–1473. https://doi.org/10.1038/nn.4658

Eichenbaum, H. (2017). On the integration of space, time, and memory. *Neuron*, *95*(5), 1007–1018. https://doi.org/10.1016/j.neuron.2017.06.036

Epstein, R. A. (2008). Parahippocampal and retrosplenial contributions to human spatial navigation. *Trends in Cognitive Sciences*, *12*(10), 388–396. https://doi.org/10.1016/j.tics.2008.07.004

Favre, G., Banta Lavenex, P., & Lavenex, P. (2012a). Developmental regulation of expression of schizophrenia susceptibility genes in the primate hippocampal formation. *Translational Psychiatry*, *2*, e173. https://doi.org/10.1038/tp.2012.105

Favre, G., Banta Lavenex, P., & Lavenex, P. (2012b). miRNA regulation of gene expression: A predictive bioinformatics analysis in the postnatally developing monkey hippocampus. *PLoS One*, *7*(8), e43435. https://doi.org/10.1371/journal.pone.0043435

Gatome, C. W., Slomianka, L., Lipp, H. P., & Amrein, I. (2010). Number estimates of neuronal phenotypes in layer II of the medial entorhinal cortex of rat and mouse. *Neuroscience*, *170*(1), 156–165. https://doi.org/10.1016/j.neuroscience.2010.06.048

Grateron, L., Cebada-Sanchez, S., Marcos, P., Mohedano-Moriano, A., Insausti, A. M., Munoz, M., … Insausti, R. (2003). Postnatal development of calcium-binding proteins immunoreactivity (parvalbumin, calbindin, calretinin) in the human entorhinal cortex. *Journal of Chemical Neuroanatomy*, *26*(4), 311–316.

Gundersen, H. J. (1988). The nucleator. *Journal of Microscopy*, *151*(Pt 1), 3–21.

Huttenlocher, P. R., & Dabholkar, A. S. (1997). Regional differences in synaptogenesis in human cerebral cortex. *The Journal of Comparative Neurology*, *387*(2), 167–178. https://doi.org/10.1002/(sici)1096-9861(19971020)387:2<167::aid-cne1>3.0.co;2-z

Insausti, R., & Amaral, D. G. (2008). Entorhinal cortex of the monkey: IV. Topographical and laminar organization of cortical afferents. *The Journal of Comparative Neurology*, *509*(6), 608–641. https://doi.org/10.1002/cne.21753

Insausti, R., Amaral, D. G., & Cowan, W. M. (1987). The entorhinal cortex of the monkey: II. Cortical afferents. *The Journal of Comparative Neurology*, *264*(3), 356–395.

Jabès, A., Banta Lavenex, P., Amaral, D. G., & Lavenex, P. (2010). Quantitative analysis of postnatal neurogenesis and neuron number in the macaque monkey dentate gyrus. *The European Journal of Neuroscience*, *31*(2), 273–285. https://doi.org/10.1111/j.1460-9568.2009.07061.x

Jabès, A., Banta Lavenex, P., Amaral, D. G., & Lavenex, P. (2011). Postnatal development of the hippocampal formation: A stereological study in macaque monkeys. *The Journal of Comparative Neurology*, *519*(6), 1051–1070. https://doi.org/10.1002/cne.22549

Kesner, R. P. (2013). An analysis of the dentate gyrus function. *Behavioural Brain Research*, *254*, 1–7. https://doi.org/10.1016/j.bbr.2013.01.012

Kesner, R. P., Lee, I., & Gilbert, P. (2004). A behavioral assessment of hippocampal function based on a subregional analysis. *Reviews in the Neurosciences*, *15*(5), 333–351.

Kesner, R. P., & Rolls, E. T. (2015). A computational theory of hippocampal function, and tests of the theory: New developments. *Neuroscience and Biobehavioral Reviews*, *48*, 92–147. https://doi.org/10.1016/j.neubiorev.2014.11.009

Knierim, J. J., & Neunuebel, J. P. (2016). Tracking the flow of hippocampal computation: Pattern separation, pattern completion, and attractor dynamics. *Neurobiology of Learning and Memory*, *129*, 38–49. https://doi.org/10.1016/j.nlm.2015.10.008

Knierim, J. J., Neunuebel, J. P., & Deshmukh, S. S. (2014). Functional correlates of the lateral and medial entorhinal cortex: Objects, path integration and local-global reference frames. *Philosophical Transactions of the Royal Society of London. Series B, Biological Sciences*, *369*(1635), 20130369. https://doi.org/10.1098/rstb.2013.0369

Kobayashi, Y., & Amaral, D. G. (2003). Macaque monkey retrosplenial cortex: II. Cortical afferents. *The Journal of Comparative Neurology*, *466*(1), 48–79. https://doi.org/10.1002/cne.10883

Kobayashi, Y., & Amaral, D. G. (2007). Macaque monkey retrosplenial cortex: III. Cortical efferents. *The Journal of Comparative Neurology*, *502*(5), 810–833. https://doi.org/10.1002/cne.21346

Kuruvilla, M. V., & Ainge, J. A. (2017). Lateral entorhinal cortex lesions impair local spatial frameworks. *Frontiers in Systems Neuroscience*, *11*, 1-12. https://doi.org/10.3389/fnsys.2017.00030

Langston, R. F., Ainge, J. A., Couey, J. J., Canto, C. B., Bjerknes, T. L., Witter, M. P., … Moser, M. B. (2010). Development of the spatial representation system in the rat. *Science*, *328*(5985), 1576–1580.

Lavenex, P., & Amaral, D. G. (2000). Hippocampal-neocortical interaction: A hierarchy of associativity. *Hippocampus*, *10*(4), 420–430. https://doi.org/10.1002/1098-1063(2000)10:4<420::AID-HIPO8>3.0.CO;2-5

Lavenex, P., & Banta Lavenex, P. (2013). Building hippocampal circuits to learn and remember: Insights into the development of human memory. *Behavioural Brain Research*, *254*, 8–21. https://doi.org/10.1016/j.bbr.2013.02.007

Lavenex, P., Banta Lavenex, P., & Amaral, D. G. (2004). Non-phosphorylated high-molecular-weight neurofilament expression suggests early maturation of the monkey subiculum. *Hippocampus*, *14*(7), 797–801. https://doi.org/10.1002/hipo.20028

Lavenex, P., Banta Lavenex, P., & Amaral, D. G. (2007). Postnatal development of the primate hippocampal formation. *Developmental Neuroscience*, *29*(1–2), 179–192. https://doi.org/10.1159/000096222

Lavenex, P., Banta Lavenex, P., Bennett, J. L., & Amaral, D. G. (2009). Postmortem changes in the neuroanatomical characteristics of the primate brain: Hippocampal formation. *The Journal of Comparative Neurology*, *512*(1), 27–51. https://doi.org/10.1002/cne.21906

Lavenex, P., Banta Lavenex, P., & Favre, G. (2014). What animals can teach clinicians about the hippocampus. *Frontiers of Neurology and Neuroscience*, *34*, 36–50. https://doi.org/10.1159/000356418

Lavenex, P., Sugden, S. G., Davis, R. R., Gregg, J. P., & Lavenex, P. B. (2011). Developmental regulation of gene expression and astrocytic processes may explain selective hippocampal vulnerability. *Hippocampus*, *21*(2), 142–149. https://doi.org/10.1002/hipo.20730

Newcombe, N. S., Huttenlocher, J., Bullock Drummey, A., & Wiley, J. G. (1998). The development of spatial location coding: Place learning and dead reckoning in the second and third years. *Cognitive Development*, *13*, 185–200.

Nilssen, E. S., Doan, T. P., Nigro, M. J., Ohara, S., & Witter, M. P. (2019). Neurons and networks in the entorhinal cortex: A reappraisal of the lateral and medial entorhinal subdivisions mediating parallel cortical pathways. *Hippocampus*, *29*, 1238–1254. https://doi.org/10.1002/hipo.23145

Nowakowski, R. S., & Rakic, P. (1981). The site of origin and route and rate of migration of neurons to the hippocampal region of the rhesus monkey. *The Journal of Comparative Neurology*, *196*(1), 129–154.

Ohara, S., Gianatti, M., Itou, K., Berndtsson, C. H., Doan, T. P., Kitanishi, T., … Witter, M. P. (2019). Entorhinal layer II calbindin-expressing neurons originate widespread telencephalic and intrinsic projections. *Frontiers in Systems Neuroscience*, *13*, 54. https://doi.org/10.3389/fnsys.2019.00054

Peck, J. R., & Taube, J. S. (2017). The postrhinal cortex is not necessary for landmark control in rat head direction cells. *Hippocampus*, *27*(2), 156–168. https://doi.org/10.1002/hipo.22680

Piguet, O., Chareyron, L. J., Banta Lavenex, P., Amaral, D. G., & Lavenex, P. (2018). Stereological analysis of the rhesus monkey entorhinal cortex. *The Journal of Comparative Neurology*, *526*(13), 2115–2132. https://doi.org/10.1002/cne.24496

Pitkänen, A., Kelly, J. L., & Amaral, D. G. (2002). Projections from the lateral, basal, and accessory basal nuclei of the amygdala to the entorhinal cortex in the macaque monkey. *Hippocampus*, *12*(2), 186–205.

Rabinowicz, T., Petetot, J. M., Khoury, J. C., & de Courten-Myers, G. M. (2009). Neocortical maturation during adolescence: change in neuronal soma dimension. *Brain and Cognition*, *69*(2), 328–336. https://doi.org/10.1016/j.bandc.2008.08.005

Rakic, P., Bourgeois, J. P., Eckenhoff, M. F., Zecevic, N., & Goldman-Rakic, P. S. (1986). Concurrent overproduction of synapses in diverse regions of the primate cerebral cortex. *Science*, *232*(4747), 232–235. https://doi.org/10.1126/science.3952506

Rakic, P., & Nowakowski, R. S. (1981). The time of origin of neurons in the hippocampal region of the rhesus monkey. *Journal of Comparative Neurology*, *196*(1), 99–128.

Ribordy, F., Jabès, A., Banta Lavenex, P., & Lavenex, P. (2013). Development of allocentric spatial memory abilities in children from 18 months to 5 years of age. *Cognitive Psychology*, *66*(1), 1–29. https://doi.org/10.1016/j.cogpsych.2012.08.001

Ribordy Lambert, F., Lavenex, P., & Banta Lavenex, P. (2015). Improvement of allocentric spatial memory resolution in children from 2 to 4 years of age. *International Journal of Behavioral Development*, *39*(4), 318–331. https://doi.org/10.1177/0165025415584808

Ribordy Lambert, F., Lavenex, P., & Banta Lavenex, P. (2016). The "when" and the "where" of single-trial allocentric spatial memory performance in young children: Insights into the development of episodic memory. *Developmental Psychobiology*, *59*(2), 185–196.

Rieser, J. J., & Heiman, M. L. (1982). Spatial self-reference systems and shortest-route behavior in toddlers. *Child Development*, *53*, 524–533.

Savelli, F., & Knierim, J. J. (2019). Origin and role of path integration in the cognitive representations of the hippocampus: Computational insights into open questions. *Journal of Experimental Biology*, *222*(Pt Suppl. 1), 1-13. https://doi.org/10.1242/jeb.188912

Schwartz, S. P., & Coleman, P. D. (1981). Neurons of origin of the perforant path. *Experimental Neurology*, *74*(1), 305–312. https://doi.org/10.1016/0014-4886(81)90169-2

Surmeli, G., Marcu, D. C., McClure, C., Garden, D. L. F., Pastoll, H., & Nolan, M. F. (2015). Molecularly defined circuitry reveals input-output segregation in deep layers of the medial entorhinal cortex. *Neuron*, *88*(5), 1040–1053. https://doi.org/10.1016/j.neuron.2015.10.041

Suzuki, W. A., & Amaral, D. G. (1994). Topographic organization of the reciprocal connections between the monkey entorhinal cortex and the perirhinal and parahippocampal cortices. *Journal of Neuroscience*, *14*(3), 1856–1877.

Suzuki, W. A., Miller, E. K., & Desimone, R. (1997). Object and place memory in the macaque entorhinal cortex. *Journal of Neurophysiology*, *78*(2), 1062–1081 Retrieved from < Go to ISI>://A1997XT27300041.

Taube, J. S. (2007). The head direction signal: Origins and sensory-motor integration. *Annual Review of Neuroscience*, *30*, 181–207. https://doi.org/10.1146/annurev.neuro.29.051605.112854

Tsao, A., Sugar, J., Lu, L., Wang, C., Knierim, J. J., Moser, M. B., & Moser, E. I. (2018). Integrating time from experience in the lateral entorhinal cortex. *Nature*, *561*(7721), 57. https://doi.org/10.1038/s41586-018-0459-6

West, M. J., Slomianka, L., & Gundersen, H. J. (1991). Unbiased stereological estimation of the total number of neurons in thesubdivisions of the rat hippocampus using the optical fractionator. *The Anatomical Record*, *231*(4), 482–497.

Witter, M. P., & Amaral, D. G. (1991). Entorhinal cortex of the monkey: V. projections to the dentate gyrus, hippocampus, and subicular complex. *The Journal of Comparative Neurology*, *307*(3), 437–459.

Witter, M. P., Doan, T. P., Jacobsen, B., Nilssen, E. S., & Ohara, S. (2017). Architecture of the entorhinal cortex: A review of entorhinal anatomy in rodents with some comparative perspective. *Frontiers in Systems Neuroscience*, *11*, 1-12. https://doi.org/10.3389/fnsys.2017.00046

Witter, M. P., & Moser, E. I. (2006). Spatial representation and the architecture of the entorhinal cortex. *Trends in Neurosciences*, *29*(12), 671–678. https://doi.org/10.1016/j.tins.2006.10.003

Witter, M. P., Van Hoesen, G. W., & Amaral, D. G. (1989). Topographical organization of the entorhinal projection to the dentate gyrus of the monkey. *The Journal of Neuroscience*, *9*(1), 216–228.

Yoder, R. M., Peck, J. R., & Taube, J. S. (2015). Visual landmark information gains control of the head direction signal at the lateral mammillary nuclei. *Journal of Neuroscience*, *35*(4), 1354–1367. https://doi.org/10.1523/Jneurosci.1418-14.2015